CHAPTER 5 PERFORMANCE OF AN EMULSION TREATED GRAVEL UNDER LABORATORY AND HVS TESTING

5.1 INTRODUCTION

The experimental programme in this study was developed to provide an understanding of the structural behaviour and the engineering properties that influence the structural behaviour of materials treated with bitumen emulsion and cement. Data acquired from the study was used to develop a failure criteria and subsequent transfer functions for emulsion treated materials. The tests consisted of laboratory testing and testing under the Heavy Vehicle Simulator (HVS).

The laboratory testing included an investigation of different contents of cement and bitumen emulsion on the engineering properties as well as the behaviour under static and dynamic triaxial testing. Different bitumen and cement contents were considered in an attempt to provide a classification for emulsion treated material and to define the structural input parameters into the structural design process.

The HVS tests were full-scale tests on an in-service pavement. The HVS tests provided information on the possible modes of distress under HVS testing as well as the behaviour of the emulsion treated materials in the "pre-cracked" and "post-cracked" phases under various wheel loads.

5.2 EXPERIMENTAL DESIGN

5.2.1 Laboratory testing

The following tests were conducted on the material treated with various cement and binder contents:

- California Bearing Ratio tests (CBR)
- Unconfined Compressive tests (UCS)
- Indirect Tensile tests (ITS)
- Static four point flexural beam tests
- Drained unconsolidated static triaxial tests
- Drained unconsolidated dynamic triaxial tests

The UCS, ITS and flexural beam tests were conducted at cement contents of 0, 1 and 2% and net bitumen contents of 0, 0.6, 1.8 and 3%. A minimum of three repetitions for the CBR, UCS and ITS were performed with a minimum number of 4 repetitions for the flexural beam test. Table 5.1 presents a detailed overview of the experimental design for the laboratory testing.

Table 5.1 Tests on different combinations of cement and net bitumen contents

Cement content (%)	Net bitumen content (%) 0	0.6	1.8	3.0
0	CBR	CBR, UCS, ITS, Flexural beam	CBR, UCS, ITS, Flexural beam	CBR, UCS, ITS, Flexural beam
1	UCS, ITS, Flexural beam	UCS, ITS, Flexural beam	UCS, ITS, Flexural beam	UCS, ITS, Flexural beam
2	UCS, ITS, Flexural beam, Dynamic triaxial, Static triaxial	-	UCS, ITS, Flexural beam, Dynamic triaxial, Static triaxial, HVS	UCS, ITS, Flexural beam

The static and dynamic triaxial tests were performed at two densities, namely 67% and 73% relative density and at saturation levels of 75% and 45%. For the static triaxial tests confining pressures of 20 kPa, 80 kPa, 140 kPa and 200 kPa were used for each saturation and density level. The dynamic tests were performed at confining pressures of 80 kPa and 140 kPa and at stress ratios of 0.2, 0.55 and 0.9.

The bitumen and cement content for all the static and dynamic triaxial tests were kept at 1.8 % and 2 % respectively, which were the same as used on the HVS site.

The aim of this testing was to determine the influence of different cement and net bitumen contents on some engineering properties. The values reported for the CBR, UCS and ITS are not recommended for use as guidelines in the design of emulsion treated materials and only illustrate the effect of cement and emulsion on them.

Specimen preparation and curing

The mixing process of the cement and bitumen emulsion was not part of this research and mixing was done by hand in the laboratory. All the samples were cured for 28 days at ambient temperature. Different curing methods and curing periods were not considered in this study. This was done in detail by Verhaeghe et al (1998). The curing time and method decided upon was done to enable results from this study to be compared with the results from other studies undertaken on foamed bitumen. (Long: 2001, Robroch: 2001). All the samples for the CBR, UCS, ITS and Flexural beam tests were compacted to 100% of modified AASHTO density, and tested at optimum moisture content.

5.2.2 Laboratory test procedures

California Bearing Ratio (CBR)

The California Bearing Ratio (CBR) was developed to describe the bearing capacity of a material or soil. It is determined by measuring the load required to allow a standard piston to penetrate the surface of a material at a rate of 1.27 mm per minute to depths of 2.54, 5.08 and 7.62 mm. The California load standards are 13.344, 20.016 and 25.354 kN respectively for each penetrated depth.

The CBR test is described in detail as test method A8 in the TMH1 (NITRR: 1986).

Unconfined Compressive Strength Tests (UCS)

The Unconfined compressive test is used to evaluate the strength of stabilised materials in the laboratory. The UCS of a stabilised material is the load in kPa required to crush a specimen with a height of 127 mm and a diameter of 152.4 mm, to total failure, at a constant load application rate of 140 kPa per second.

The UCS test is described as test method A14 in the TMH1 (NITRR: 1986).

Indirect Tensile Strength Tests (ITS)

The Indirect tensile strength is used to evaluate the tensile strength properties of a stabilised material. The test consists of loading a cylindrical specimen with compressive loads distributed along two loading strips, on the sides of the specimen. The load is applied at a constant rate of 140 kPa per second. This results in a relatively uniform tensile stress perpendicular to, and along, the diametric plane of the applied load. Failure usually occurs by splitting along the loaded plane. The details of the test are described as test method A16T in TMH1 (NITRR: 1986).

Static four point beam test

The static four point beam test consists of a beam with dimensions of 75 * 75 * 450 mm which is supported at each edge. Vertical loads are applied at two positions at a distance equal to one third of the length of the beam, away from the end of the beam. The test is performed under controlled strain mode and the magnitude of the load is determined by the resistance of the beam as it is flexed. The vertical displacement of the beam is measured on top of the beam by two Linear Variable Displacement Transducers (LVDT's) on the middle span, halfway between the loading points. The applied load and the vertical displacement of the beam, recorded during the test, are used to calculate the horizontal stress and strain at the bottom of the beam from linear elastic beam theory.

The basic set-up of the static four-point beam test is illustrated in the photograph in Figure 5.1 and a typical example of the stress-strain response measured during the test is shown in Figure 5.2.

Figure 5.1 Typical set-up of the four point static beam test.

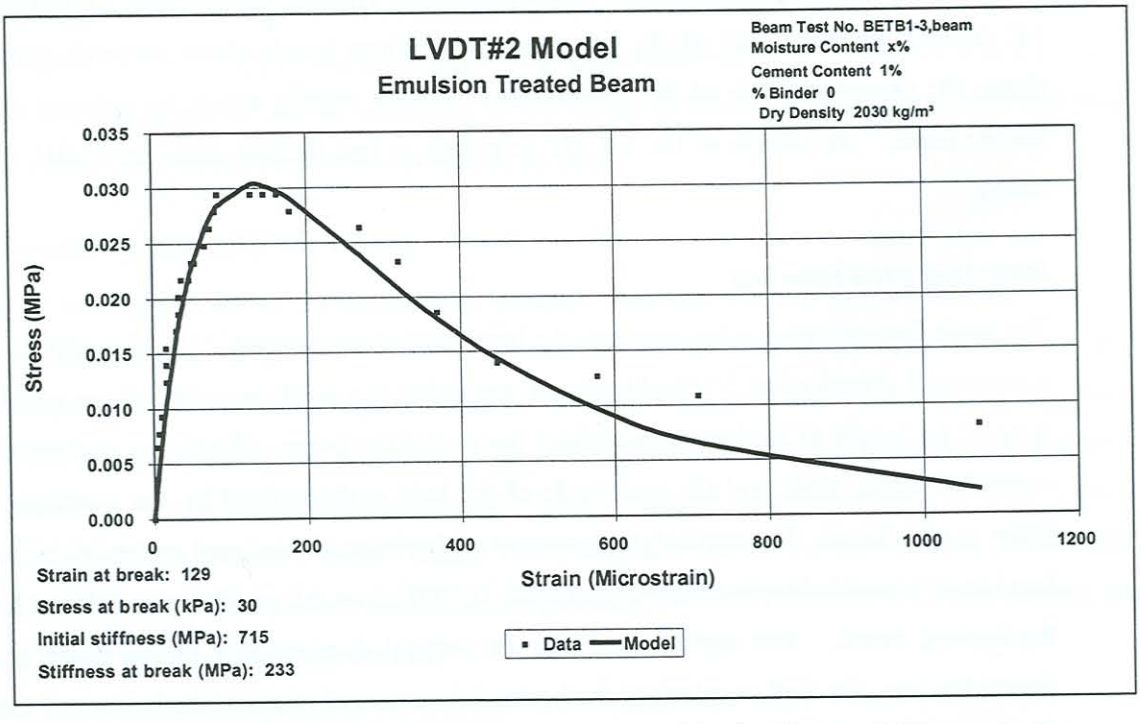

Figure 5.2 Typical Stress-Strain response measured during four-point beam test.

Static triaxial tests

The static triaxial test is widely used to determine the shear strength parameters of soils. In this test, samples of up to 150 mm in diameter and 300 mm in height can be used. The sample is encased by a thin rubber membrane and placed inside a plastic cylindrical chamber that may be filled with water or compressed air to provide a confining pressure. To cause the shear failure of the sample, axial stress is applied through a hydraulic loading ram from the top. A load cell in the loading ram records the applied load, while a LVDT in the loading ram records the displacement of the ram.

The load is applied at a constant rate of 2 mm per minute and the magnitude of the load and displacement of the loading is recorded electronically. The recorded load and displacement may be used to calculate the deviator stress (σ_1 - σ_3) applied to the sample and the vertical uniaxial strain of the sample. A typical stress-strain curve from a static triaxial test is shown in Figure 5.3a. The data obtained from the stress-strain plot may then be used to calculate the slope of the stress-strain curve that is the secant stiffness modulus (E_{sec}) of the sample (Figure 5.3b).

The static triaxial test is better known for determining the shear strength envelope or Möhr-Coulomb failure envelope of granular materials (Das: 1990). This is done by performing a number of static triaxial tests at different confining pressures. The peak stress (yield stress) that a sample can sustain, at a particular confining pressure is obtained from the turning point on the stress-strain curve. By plotting the Möhr stress circles associated with the different confining pressures and respective yield stress values, a failure envelope may be obtained from the tangent drawn to the Möhr stress circles. The shear strength parameters, c and ϕ, may then be determined from the Möhr stress circles.

Dynamic triaxial tests

The dynamic triaxial test is a repeated load test, where a load pulse with a magnitude below the static shear strength of the material is repeatedly applied to the sample with a short rest period between the pulses. The set-up of the dynamic triaxial test is similar to that of the static triaxial test, with the addition of a set of LVDT's that are normally fixed over the middle third of the height of the sample. The elastic and plastic deformation over the middle third of the sample can then be measured. This eliminates the influence of frictional shear forces and edge displacement effects between the load plates and the sample.

STATIC TRIAXIAL TEST

Material: Ferricrete **Emulsion**

Sample #: ETF01

Dry Density (kg/cub m): 1870 **Confining pressure (kPa): 22**

Moisture (%): 10.5 **Linear stiffness (MPa): 474**

Maximum deviator stress (kPa): 1998

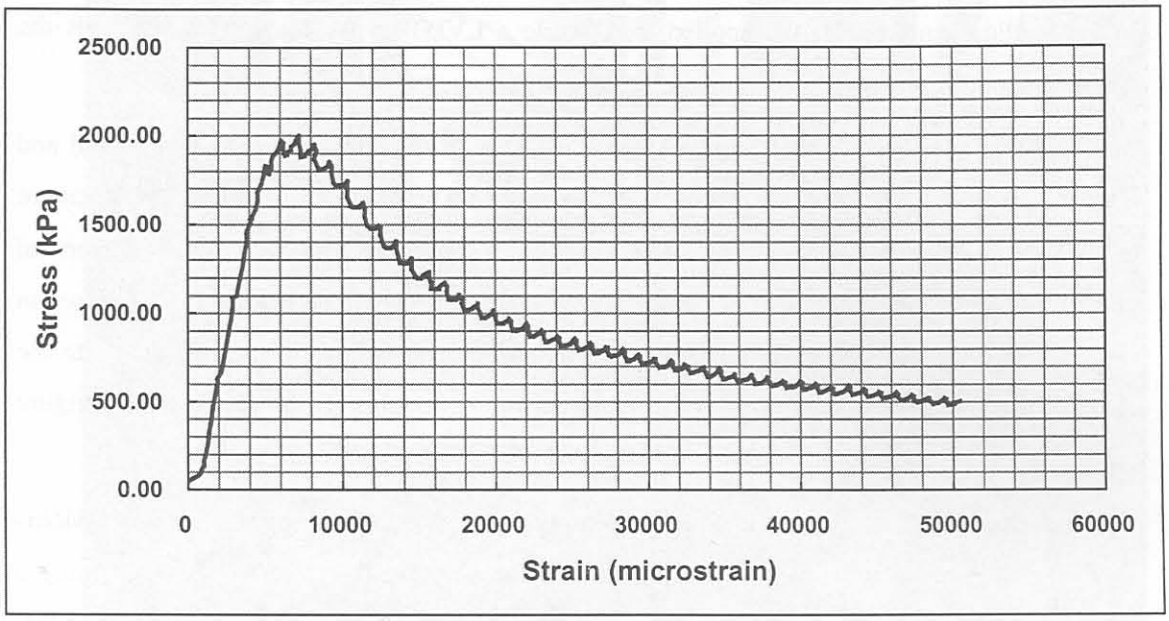

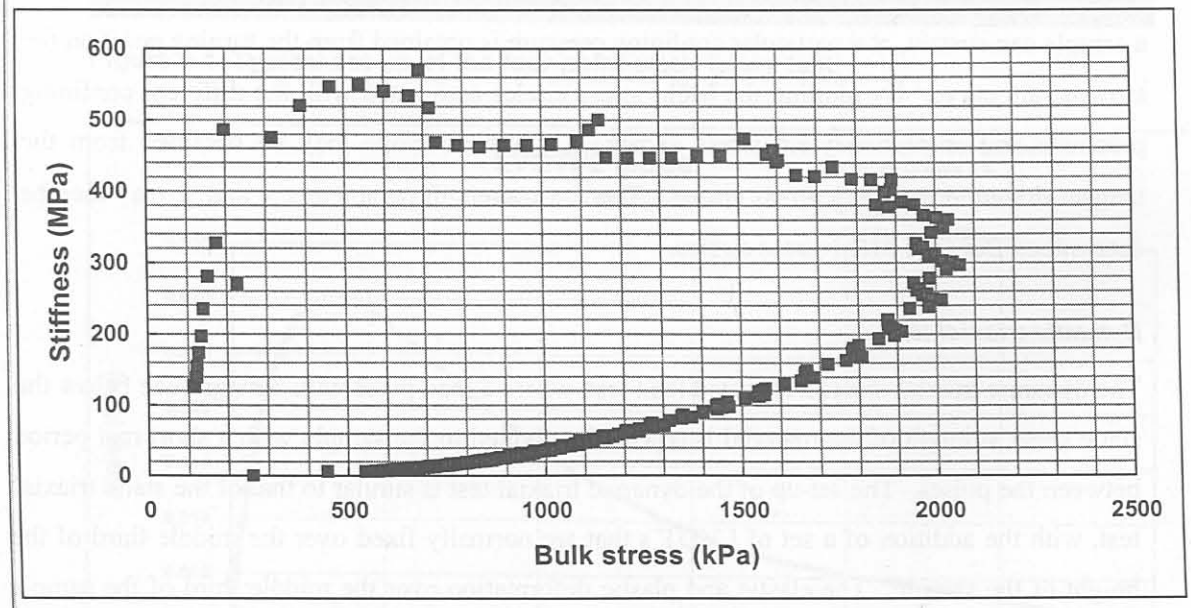

Figure 5.3 Typical result from the static triaxial test.

Material: Ferricrete with cement **Sample #:** ETF19
Density: 2062 kg/ cub m **Confining pressure:** 80.8 kPa
Moisture: 10.7 % **Stress Ratio** 90 % of failure stress

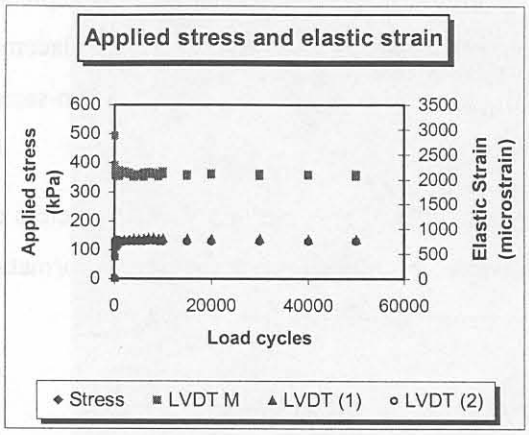

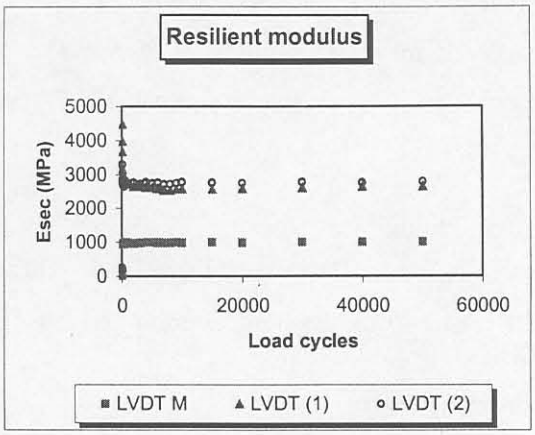

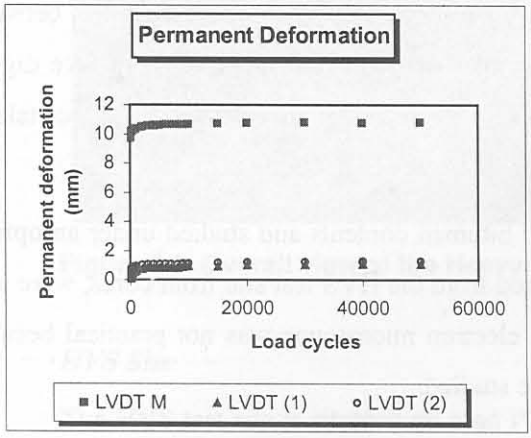

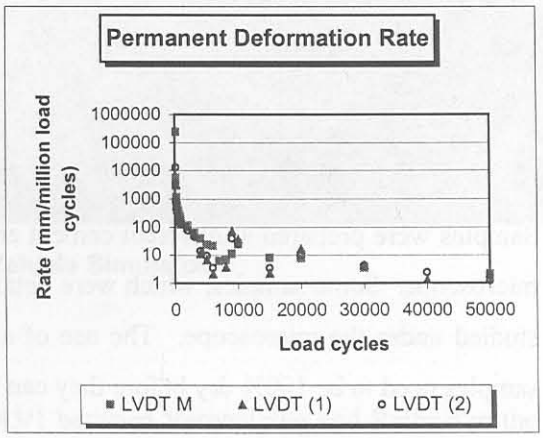

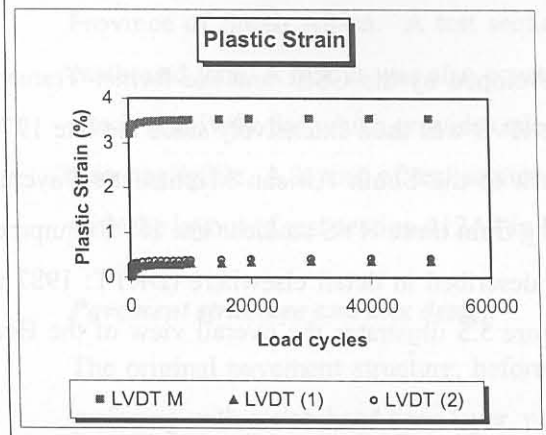

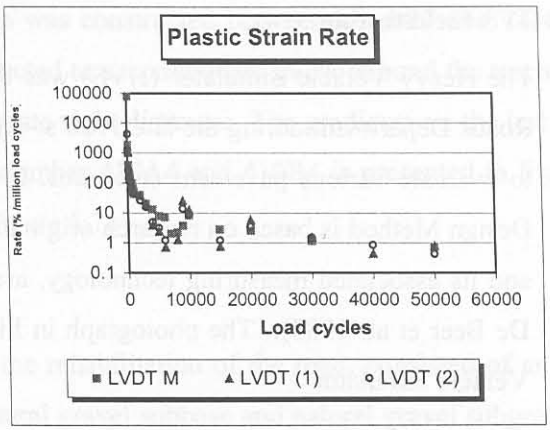

	Elastic response results				Plastic response results			
	Average for test		Final values		Final values			
	Elastic Strain (microstrain)	Resilient Modulus (MPa)	Elastic Strain (microstrain)	Resilient Modulus (MPa)	Permanent Deformation (mm)	Rate of PD (mm/million)	Plastic Strain (%)	Rate of PS (%/million)
LVDT M	2127	939	2065	1004	10.78	2.1	3.55	0.7
LVDT #1	726	2667	786	2639	1.10	2.2	0.37	0.8
LVDT #2	722	2659	748	2773	1.28	1.2	0.43	0.4
	724	2663	767	2706	4.38	1.8	1.45	0.6

Figure 5.4 Typical calculated results from a set of dynamic triaxial data

A cyclic load with a load- and rest period duration of 0.2 seconds each was selected for this study. The load magnitude for the dynamic tests was set at different levels of the maximum static load and run for 50 000 load cycles. The load-displacement response of the sample was recorded in windows of three load cycles during various stages of the test. Displacement measurements were taken from the LVDT on the loading ram as well as the two on-sample LVDT's.

By combining all the data sampled during a dynamic triaxial test, a number of parameters can be calculated, as shown in Figure 5.4. These parameters include the permanent deformation, the elastic strain, resilient modulus and rate of permanent deformation.

5.2.3 Optical microscope

The microscope consists of an ordinary optical microscope capable of magnifications between 7x and 90x. A digital camera, attached to the microscope, makes it possible to take digital pictures of the samples that are studied. State of the art software provides the feature of taking optical digital pictures at high magnification, which are perfectly in focus.

Samples were prepared at different cement and bitumen contents and studied under an optical microscope. Some samples, which were obtained from the HVS test site from cores, were also studied under the microscope. The use of an electron microscope was not practical because samples need to be 100% dry before they can be studied.

5.2.4 HVS Field testing

The Heavy Vehicle Simulator (HVS) was developed by the CSIR and the former Transvaal Roads Department during the late 1970's. The HVS was used extensively since the late 1970's to evaluate various pavement structures. Much of the South African Mechanistic Pavement Design Method is based on research originating from these HVS studies. The HVS equipment, and its associated measuring technology, are described in detail elsewhere (DRTT: 1987 and De Beer et at: 1988). The photograph in Figure 5.5 illustrates the overall view of the Heavy Vehicle Simulator.

HVS tests on emulsion treated materials were previously undertaken on labour intensive constructed pavements near Cullinan in the Gauteng Province (Mancotywa: 2000(a), 2001). The use of Deep In-Situ Recycling equipment in Southern Africa has become more popular recently for a number of reasons. Two of these reasons are the availability and cost of high quality crushed material and easier traffic accommodation. The HVS tests included in this study (test numbers 410A4, 410B4 and 412A4) were the first HVS tests performed on pavement structures treated with bitumen emulsion and cement and constructed by means of a

deep in-situ recycling machine. A Wirtgen DSR2500 deep in situ recycling machine was used in the rehabilitation of the road which was tested.

Figure 5.5 Overall view of the Heavy Vehicle Simulator

HVS Site

The HVS test site is situated on road P243/1 between Vereeniging and Balfour in the Gauteng Province of South Africa. A test section was constructed between km 14.2 and 14.4 on the eastbound lane. A detour was also constructed to accommodate traffic around the test site. The site is relatively flat which provides adequate sight distances. The gradients on the test site are also negligible. A layout of test section number 410A4 and 410B4 is presented in Figure 5.6 with the layout of test section 412A4 in Figure 5.7.

Pavement structure and mix design

The original pavement structure, before the rehabilitation of the road, consisted of an asphalt surfacing with a stabilised base layer, natural gravel subbase and natural gravel subgrade. The stabilised base layer was understood to be in an equivalent gravel phase and no longer in its fatigue life phase.

The rehabilitation design of the pavement consisted of a 30 mm Asphalt surfacing, 250 mm Deep In-Situ recycled layer stabilised with 2% cement and 1.8% net bitumen using the foam bitumen process. The lower natural gravel layers were left intact. The HVS test section consisted of a section treated with foam bitumen and a section stabilised with bitumen

emulsion. This study will focus on the tests performed on the section treated with bitumen emulsion.

A fountain on the south side of the test section, which was only discovered after the construction of the test section, resulted in the moisture content remaining high during the test. Construction related problems that could have influenced the behaviour of the test, include the presence of loose material on the base before surfacing (Semmelink and Botha: 2000a). The Asphalt surfacing was completed five days after the completion of the base layer.

Existing mix design techniques were used in the design of the emulsion treated layer. The final design however consisted of 1.8% net bitumen and 2% cement.

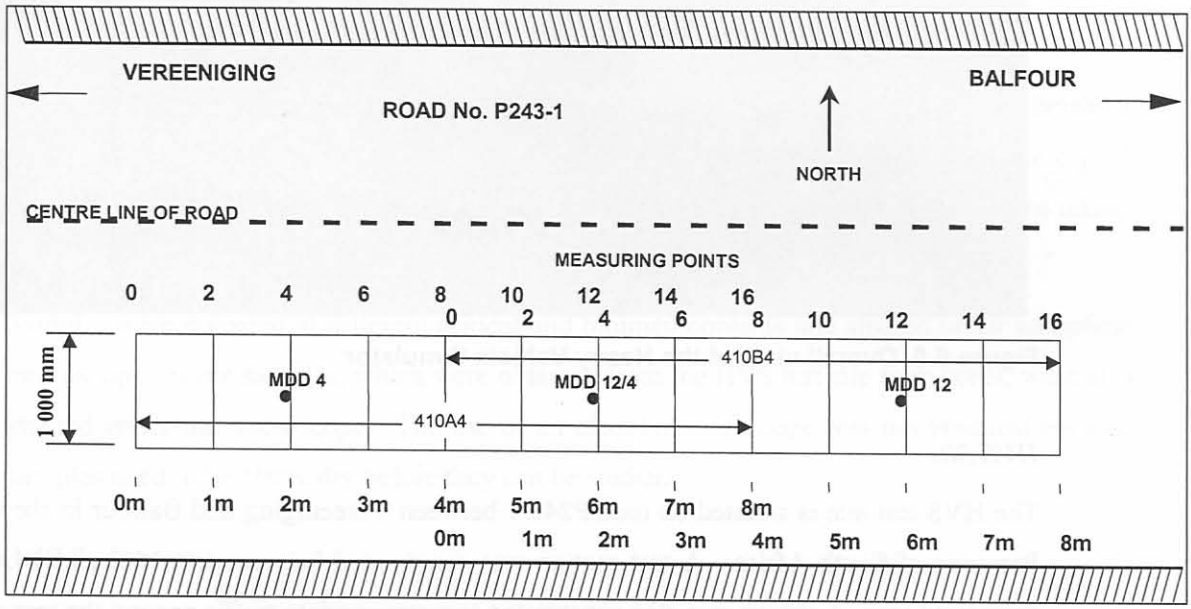

Figure 5.6 Test section layout for sections 410A4a and 410B4

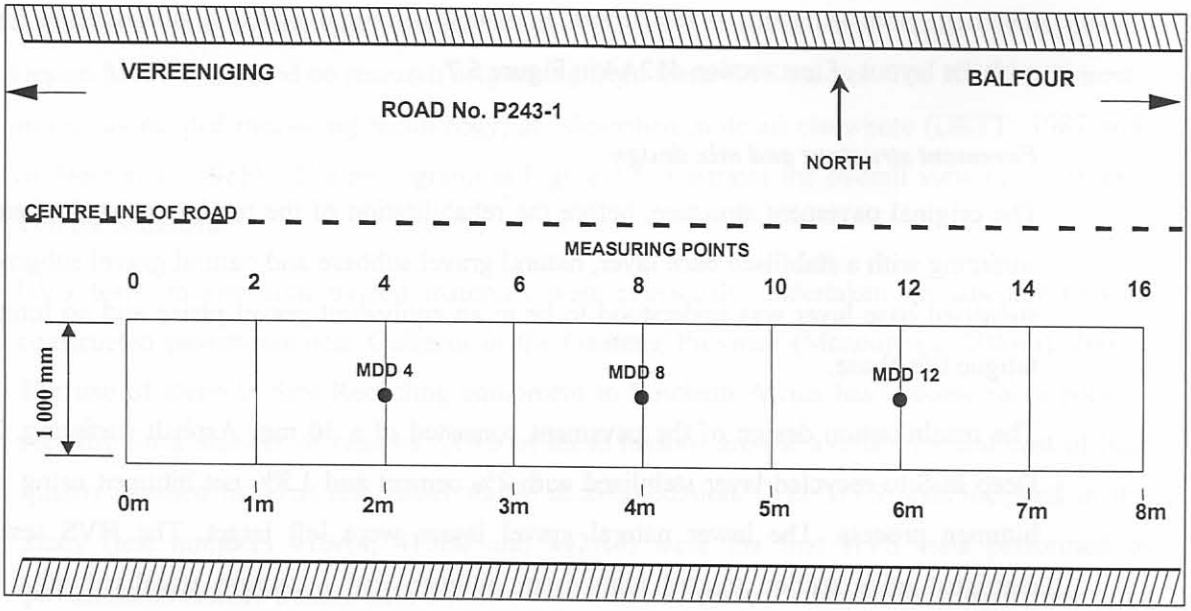

Figure 5.7 Test section layout for section 412A4A

Test programme

The test commenced with a wheel load of 80 kN and tyre inflation pressure of 800 kPa (test 410A4). A tyre inflation pressure of 800 kPa was used to ensure a homogeneous contact area between the tyre and the pavement. After 350 000 repetitions the load was increased to 100 kN and the tyre pressure to 850 kPa. The test was also moved 4 m to ensure that 4 m of the 8 m test section overlapped with 4 m of the previous test, while 4 m was on a new section (test 410B4). The 100 kN test was continued for another 150 000 repetitions after which water was applied to the surface to evaluate the behaviour of the pavement in a wet condition.

A test at the standard axle load of 40 kN (test 412A4) and tyre inflation pressure of 620 kPa was performed to evaluate the performance of the pavement under the legal axle limit as well as determine the damage factors for different distress modes of the higher wheel loads. This test was run for 957 121 repetitions where after the load was increased to 80 kN (800 kPa tyre pressure) for another 268 879 repetitions. The final 95 700 repetitions were undertaken under nominally wet conditions. The detailed test programmes of all the tests are included in Appendix C.

Table 5.2 provides a summary of the test conditions on the test sections

Table 5.2 Summary of HVS testing on sections 410A4, 410B4 and 412A4

Section	Dry/wet	Load applications	Trafficking load (kN)	Tyre inflation pressure (kPa)
410A4	Dry	295 617	80	800
410B4	Dry	171 500	100	850
	Wet	13 907	100	850
412A4	Dry	957 121	40	620
	Dry	268 879	80	800
	Wet	95 700	80	800

All three tests were performed under nominally dry conditions and no testing was permitted during rain. The load was applied at a speed of 8 km/h using a wandering pattern 1 m wide. The wandering pattern was obtained by allowing the test beam to move 50 mm sideways on a side after each load application. This process caused the wandering pattern to simulate a normal distribution of load applications on the test section as would be expected from normal traffic (Blabb and Litzka: 1995).

Pavement response measurement instruments

The standard HVS instruments were used to evaluate the performance of the test section under HVS testing. These include the following:

- Straightedge
- Laser Profilometer
- Road Surface Deflectometer (RSD)
- Multi Depth Deflectometer (MDD)
- Thermocouples

Cracks on the surface were monitored and photographed at various intervals during the test cycle. Response measurements were taken using 40 kN and 80 kN wheel loads with 620 kPa and 800 kPa tyre inflation pressure respectively. Most of the testing effort, however, was concentrated on the 40 kN measurements which were used in the analysis of the data.

5.3 THE INFLUENCE OF NET BITUMEN AND CEMENT CONTENTS ON THE STRENGTH AND FLEXIBILITY OF EMULSION TREATED GRAVEL MATERIALS

5.3.1 Materials

Ferricrete milled from the HVS test site by a Deep In-situ Recycler was used in the laboratory testing. The detailed properties of the materials are included in Appendix A. The maximum dry density of the material was approximately 2 000 kg/m^3 with an optimum moisture content of between 11.2% and 12.5%. The material has a Grading Modulus (GM) of 2.13, a Plasticity Index (PI) of 7 and a CBR of 56 at 98%, and 18 at 93% of modified AASHTO compaction. The material can be classified as a G7 material according to the TRH14 (CSRA: 1987) material classification system.

5.3.2 California Bearing Ratio

The CBR tests were performed at 100% modified AASHTO compaction with moisture content as close to the optimum moisture content as possible. The results from the CBR tests are presented in Table 5.2.

Table 5.3 Summary of California Bearing Ratio (CBR) test results (0% cement)

	Net bitumen content (%)			
	0	**0.6**	**1.8**	**3.0**
CBR @ 100%	10	13	12	25

The tested values were lower than the original tests performed on the material, and the reason for this was that the material was compacted wet of optimum in the laboratory. Compacting

the material wetter than optimum usually results in lower values even if the specimen is left in the open to dry out. Although it is not recommended that these values be used as a guideline for design, it can be seen that adding emulsion increases the bearing capacity of the material. The magnitude of this increase can however not be quantified. No reason could be obtained why the specimens were compacted wet of optimum.

5.3.3 Unconfined Compressive Strength

The UCS tests were performed at 100% modified AASHTO compaction with moisture content as close to the optimum moisture content as possible. The samples were cured for 28 days at ambient temperature and sealed to prevent excessive loss of moisture. No special or rapid curing processes were used. The results from the UCS tests are presented in Table 5.4.

Table 5.4 Summary of Unconfined Compressive Strength (UCS) test results

		Net bitumen content (%)			
		0	**0.6**	**1.8**	**3.0**
Cement	**0**	-	192	132	316
content	**1**	305	548	545	788
(%)	**2**	3 198	-	2 375	1 645

Figure 5.8 illustrates the effect of various net bitumen and cement contents on the UCS of the ferricrete material observed in this study.

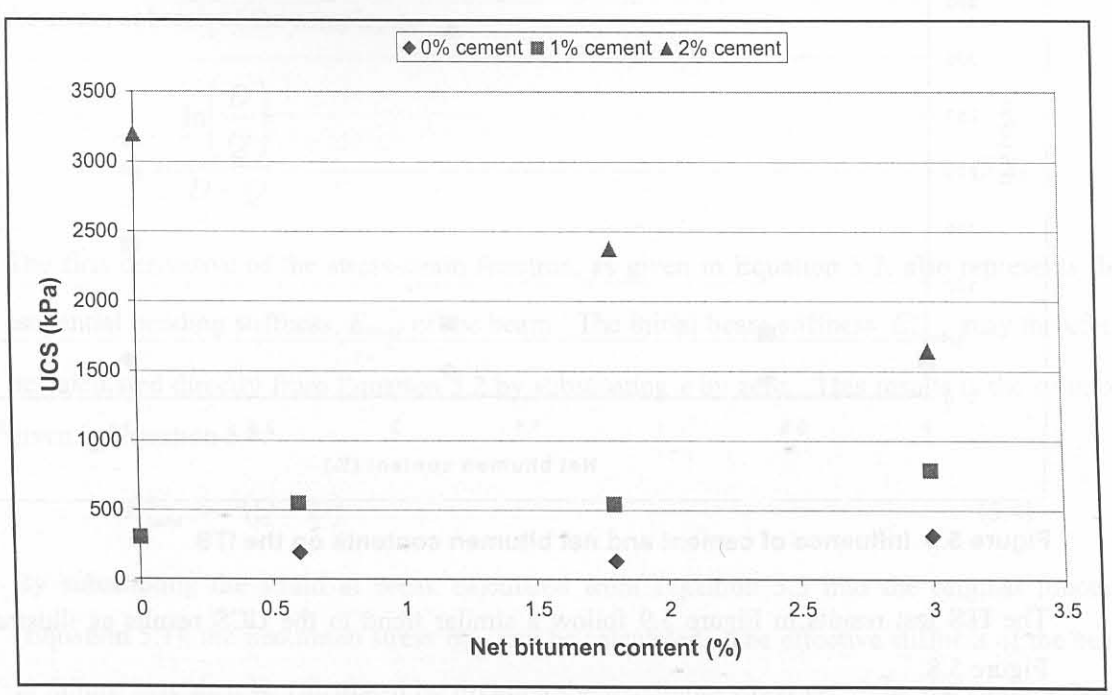

Figure 5.8 Influence of cement and net bitumen contents on the UCS

From the graph it is clear that an increase in bitumen binder has little effect on the UCS of this material at low cement content, but leads to a reduction in the UCS at higher cement content.

5.3.4 Indirect Tensile Strength

The ITS tests were also performed at 100% modified AASHTO compaction with moisture content as close to the optimum moisture content as possible. The samples were cured for 28 days at ambient temperature. The results from the ITS tests are presented in Table 5.5.

Table 5.5 Summary of Indirect Tensile Strength (ITS) test results

		Net bitumen content (%)			
		0	**0.6**	**1.8**	**3.0**
Cement	0	-	16	24	34
content	1	33	56	65	136
(%)	2	409	-	325	230

Figure 5.9 illustrates the effect of various net bitumen and cement contents on the ITS of the ferricrete material as observed in this study.

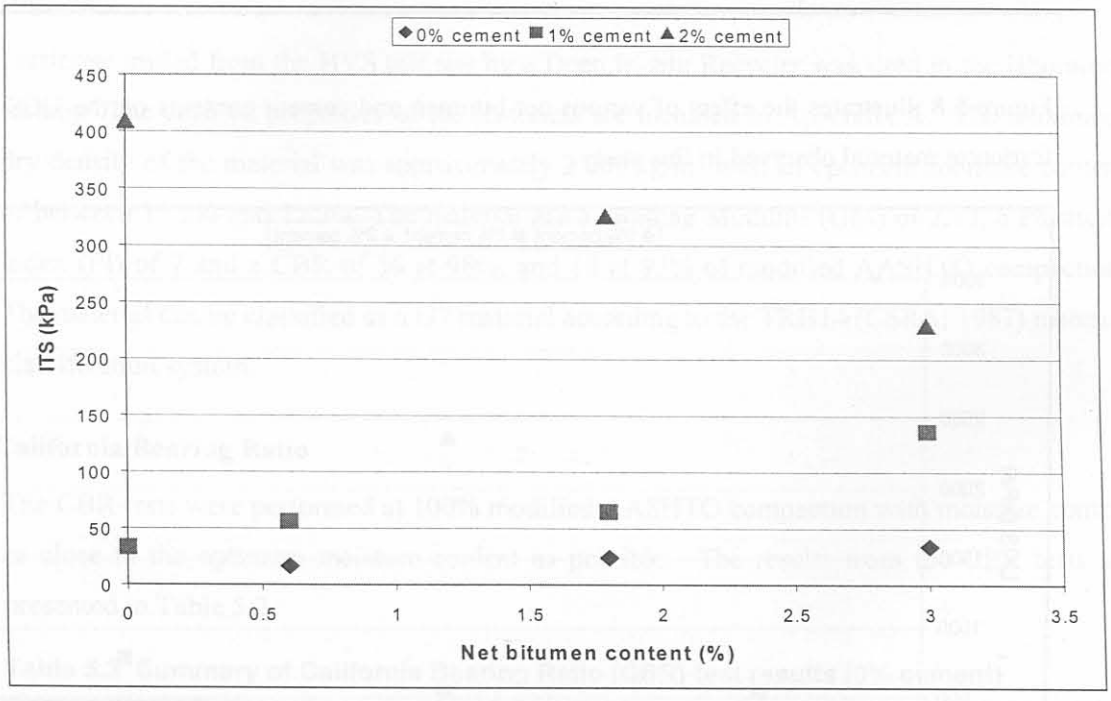

Figure 5.9 Influence of cement and net bitumen contents on the ITS

The ITS test results in Figure 5.9 follow a similar trend to the UCS results as illustrated in Figure 5.8.

5.3.5 Flexural beam tests

The data from the flexural beam test consists of a plot of stress versus strain as shown on the example in Figure 5.2. The turning point on the curve indicates failure of the specimen. The stress at this point is regarded as the stress at break while the strain at this point can be regarded as the strain at break. Theyse (2000) proposed the following mathematical model to fit the data from the beam tests:

$$\sigma = P\left(e^{-D\varepsilon} - e^{-Q\varepsilon}\right) \tag{5.1}$$

where: σ = stress

ε = strain

e = natural logarithm

P, D and Q = regression coefficients

The first derivative of the function is as follows:

$$\frac{\partial\sigma}{\partial\varepsilon} = P\left(Qe^{-Q\varepsilon} - De^{-D\varepsilon}\right) \tag{5.2}$$

The turning point of the function, where the stress is a maximum, is obtained by setting the derivative (Equation 5.2) to zero and solving for ε. The solution for ε is given in Equation 5.3 and it represents the maximum strain that can be sustained before failure of the sample and is the strain at break of the sample, ε_b.

$$\varepsilon_b = \frac{\ln\left(\frac{D}{Q}\right)}{D-Q} \tag{5.3}$$

The first derivative of the stress-strain function, as given in Equation 5.2, also represents the tangential bending stiffness, E_{bend} of the beam. The initial beam stiffness E^i_{bend} may therefore be calculated directly from Equation 5.2 by substituting ε by zero. This results is the solution given in Equation 5.4.

$$E^i_{bend} = P(Q-D) \tag{5.4}$$

By substituting the strain at break calculated from Equation 5.3 into the original function (Equation 5.1), the maximum stress σ_{max} can be calculated. The effective stiffness of the beam at failure may then be calculated by dividing the maximum stress (σ_{max}) by the strain at break (ε_b).

The amount of energy required to break the beam, that gives an indication of the toughness of the material, can be calculated by the integral of the original function between zero and the strain at break:

$$Energy = \int_0^{\varepsilon_b} \sigma \partial\varepsilon = \int_0^{\varepsilon_b} P\left(e^{-D\varepsilon} - e^{-Q\varepsilon}\right)\partial\varepsilon \tag{5.5}$$

$$= P\left(\frac{e^{-Q\varepsilon_b} - 1}{Q} - \frac{e^{-D\varepsilon_b} - 1}{D}\right) \tag{5.6}$$

Table 5.6 and Figure 5.10 to 5.12 provide a summary of the flexural beam tests.

Table 5.6 Summary of flexural beam fatigue test results

row 1 = strain at break row 2 = stress at break row 3 = toughness row 4 = Initial stiffness row 5 = Stiffness at break		Net bitumen content (%)		
		0	**1.8**	**3.0**
Cement content (%)	**0**	-	Samples broke under own weight	Samples broke under 2kg test equipment weight
	1	96 με 38 κPa 2.66 mJ/m^3 1 428 MPa 496 MPa	336 με 25 kPa 6.48 mJ/m^3 235 MPa 85 MPa	677 με 53 kPa 41.4 mJ/m^3 275 MPa 95 MPa
	2	183 με 273 kPa 45.1 mJ/m^3 4 921 MPa 1 600 MPa	141 με 360 kPa 32.2 mJ/m^3 4 731 MPa 2 655 MPa	235 με 307 kPa 53.2 mJ/m^3 3 919 MPa 2 200 MPa

The samples with no cement broke under its own weight when tested and no strain at break values could be obtained for them. The samples with only 3 % net bitumen and no cement, broke under the weight of the 2 kg test equipment, and "flowed" slowly to failure. This indicates increased flexibility at higher net bitumen content, but with little or no strength.

In general, an increase in bitumen content resulted in an increase in flexibility or strain at break. It does however not seem to have a significant effect on the stress at break. At lower cement content, an increase in bitumen content contributes positively to the amount of energy required to initiate failure.

An increase in cement content has a significant effect on the strength of the material in the sense that the stress at break increases considerably. It reduce the flexibility of the of the material, with a reduction in strain at break, when bitumen is present in the material. More energy was required to break samples with higher cement content.

An increase in the cement will therefor provide strength to the material, but adding too much will sacrifice the flexibility. This should be borne in mind when specifying the Unconfined Compressive Strength in the mix design process, and whether the objective of the structural designer is strength or flexibility.

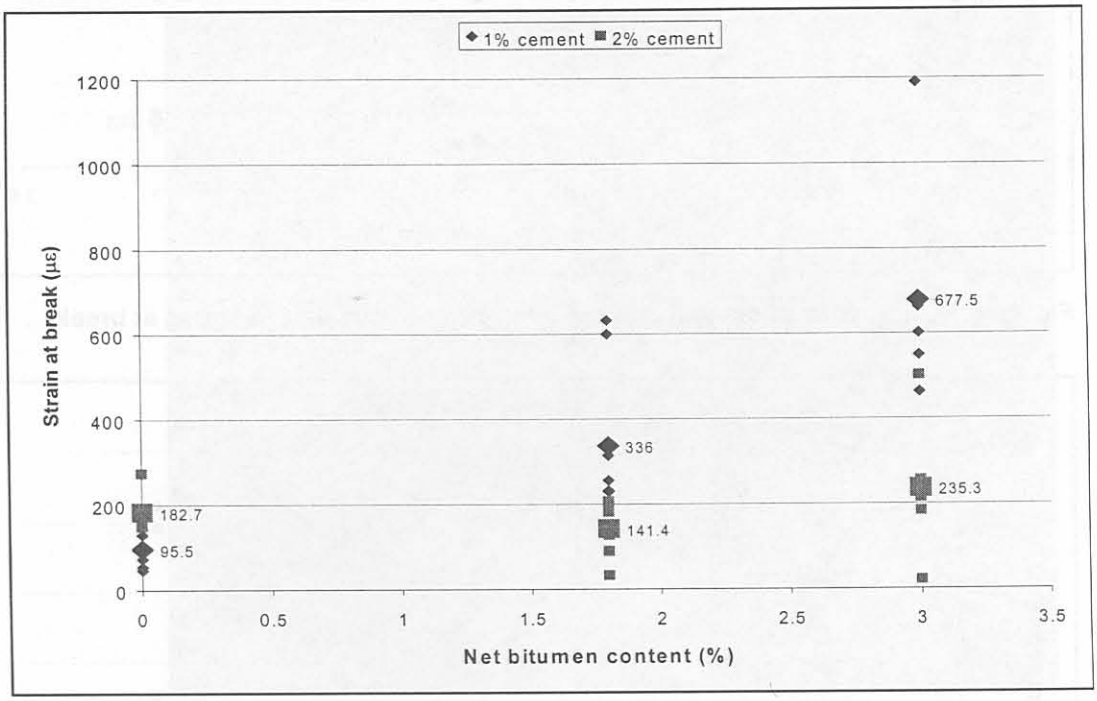

Figure 5.10 Influence of cement and net bitumen contents on the strain at break

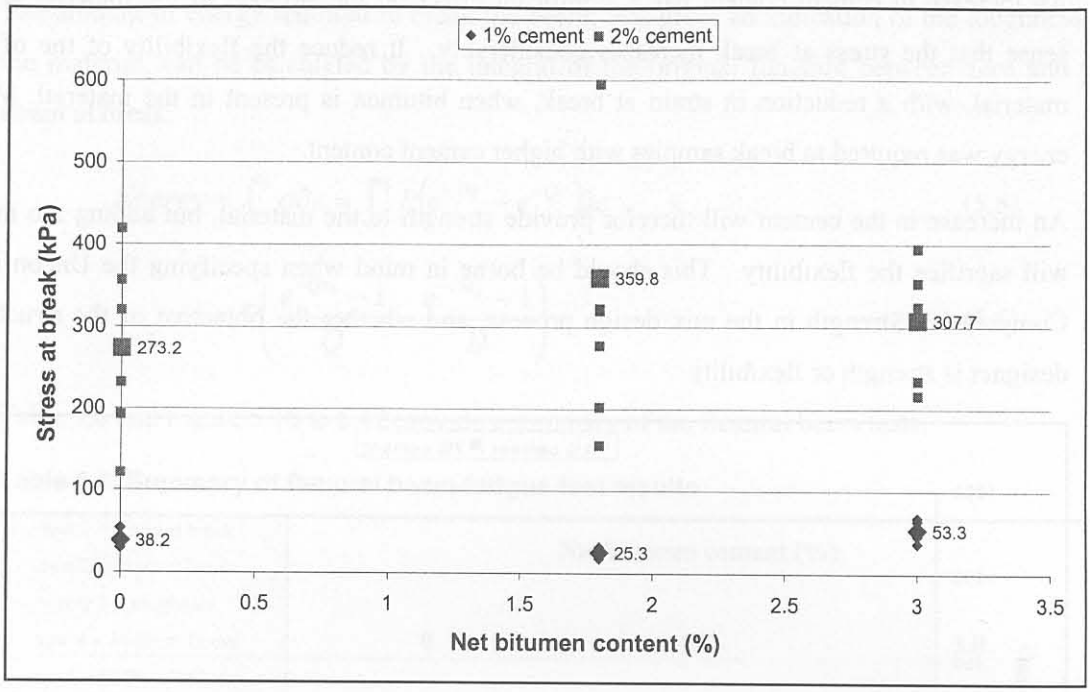

Figure 5.11 Influence of cement and net bitumen contents on the stress at break

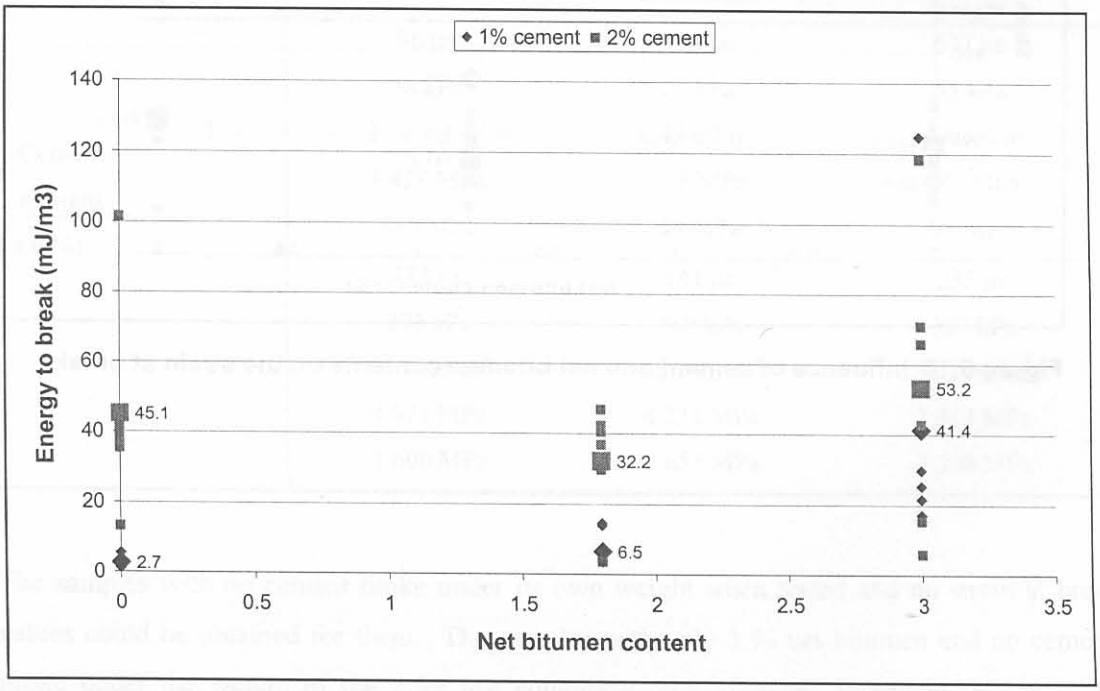

Figure 5.12 Influence of cement and net bitumen contents on the dissipated energy

5.3.6 Observations under the optical microscope

The observations under the optical microscope did not provide much more information other than the distribution of bitumen through the sample. The increased amount of bitumen present is clearly visible on the different samples, but no distinction could be made as to whether the bitumen tended to stick to the finer or coarser particles. The influence of the bitumen on the

cement particles could also not be observed. On samples from the HVS site, a film of bitumen around the larger particles was clearly visible.

Figure 5.13 presents a photograph of a laboratory sample with 2% cement and 1.8 % net bitumen under 32x magnification. The black dots on the photograph are the bitumen, with the white threads on the left of the picture, the cement. It can be seen that the bitumen is thoroughly mixed into the material. No blobs of bitumen could be observed in the samples. Figure 5.14 presents a comparison of samples with 0.6, 1.8 and 3.0 % net bitumen contents. More detailed pictures of the observations under the microscope are attached as Appendix B.

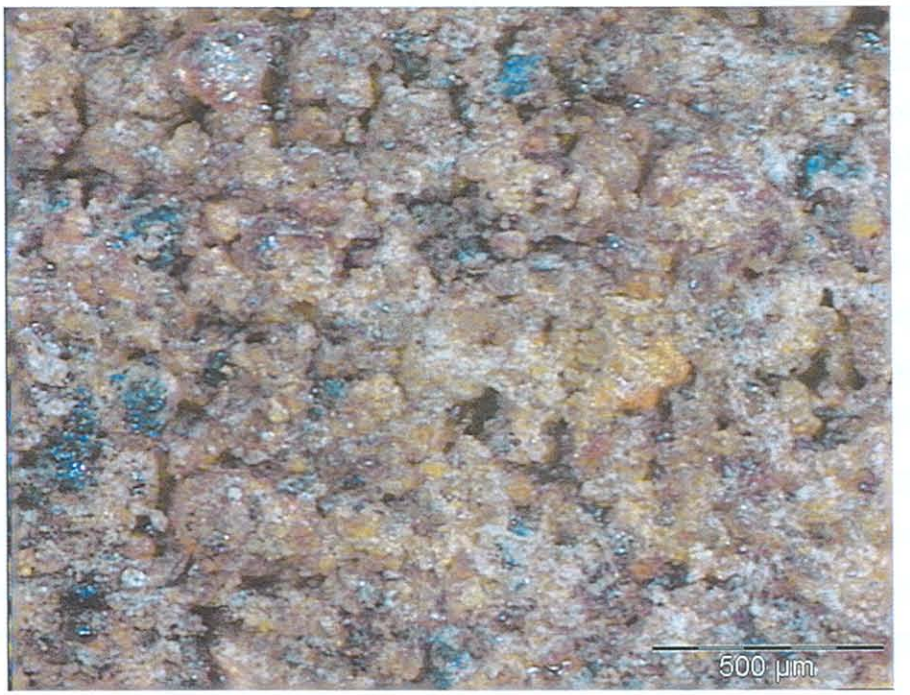

Figure 5.13 Sample from laboratory (2 % cement, 1.8 % net bitumen), 32x magnification

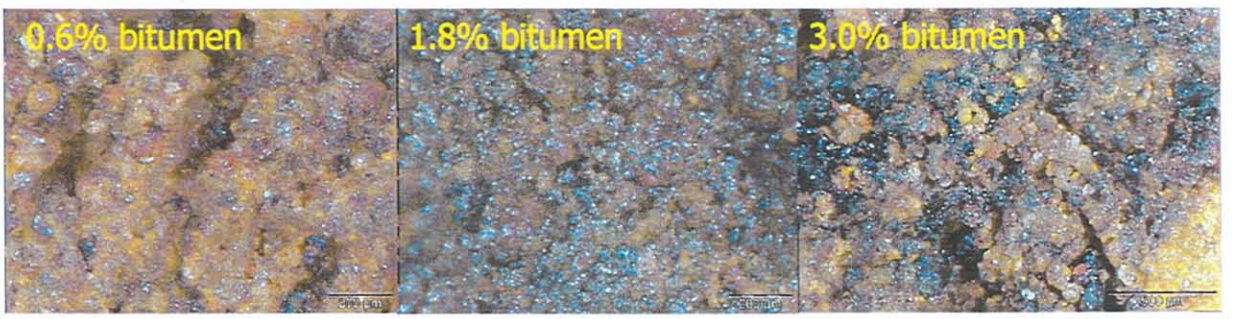

50x magnification

Figure 5.14 Optical microscope images of emulsion treated materials with different net bitumen contents (0% cement)

5.3.7 Discussion

Initial Consumption of Lime (ICL) tests on the material indicated that the ICL value of the material was 1.5 %. The ICL is an indication of the minimum amount of cement or lime that is required to satisfy conditions for the cement-hydration reaction to commence (Eades and Grimm: 1964).

From the tests done in this study it appears that the cement dominates the UCS and ITS at high cement content (above ICL) and that the addition of bituminous binder reduces the UCS and ITS of the material. At lower cement content (lower than ICL) the effect of the cement is much less and an increase in bitumen tends to have a slight increase in the UCS and/or ITS. The cement has little strengthening effect on the material when the ICL requirement is not met, and could therefore describe the greater effect of the bituminous binder on the material at low cement content. This effect could however be dependent on the type of material, but similar findings were reported to the author by Van Vuuren (2001) and Verwey (2001). An increase in binder content in excess of 3% might have a positive influence on the ITS value regardless of the cement content. The material could then behave in a visco-elastic manner with similar properties to that of asphalt materials. Additional research is however required to prove this theory.

The increase in flexibility at low cement content can be ascribed to the fact that the ICL of the material was not met and that the cement reaction, which will contribute to the brittleness of the material, has not commenced. A delicate balance between cement and bitumen content should be aimed for during the mix design process.

No comparison or relationship could be observed between the test results from the Indirect Tensile Strength and the four point flexural beam test

5.4 STATIC SHEAR STRENGTH

The static shear strength of the material was determined from static triaxial tests. The complete test results are documented by Long and Theyse (2001). Table 5.7 presents a summary of these results.

For the cement treated material, it is clear that the cohesion and friction angle is insensitive to the degree of saturation. This could be explained by the fact that the shear strength is more dependent on the chemical bonding from the cement than on the suction generated by negative pore water pressures.

Table 5.7 Static triaxial test results calculated directly from Möhr circles (Long and Theyse: 2001)

Cement content (%)	Net Bitumen content (%)	Relative density (%)	Saturation (%)	Cohesion (kPa)	Friction angle (degrees)
0	0	86	79	20	43.1
0	0	86	56	37	39.7
0	0	96	79	31	41.0
0	0	96	56	126	40.1
2	0	70	73	333	50.9
2	0	70	63	337	50.5
2	1.8	70	64	543	32.5
2	1.8	70	59	329	46.5
2	1.8	73	64	458	48.3
2	1.8	73	59	370	54.8

For the emulsion treated material it appears that the cohesion and the internal angle of friction tend to influence each other. If the cohesion increases, the internal angle of friction decreases, regardless of the increase or decrease in relative density and saturation. Due to this model effect no relationship between relative density, saturation and the two shear strength parameters could be obtained.

The values of c and ϕ can also be calculated from the K_f-line parameters a and α from a $p_f - q_f$ diagram. The relationships for c and ϕ are as follows (Lambe et al: 1996 and Das: 1990):

$$q_f = a + p_f \tan\alpha \tag{5.7}$$

$$\sin\phi = \tan\alpha \tag{5.8}$$

$$c = \frac{a}{\cos\phi} \tag{5.9}$$

where $q_f = \frac{\sigma_1 - \sigma_3}{2}$ = shear stress

$p_f = \frac{\sigma_1 + \sigma_3}{2}$ = normal stress

c = cohesion (kPa)

ϕ = angle of internal friction (degrees)

The $p_f - q_f$ diagram (Figure 5.15) is obtained from the results of static triaxial tests. A straight-line regression may be performed on the results from the maximum shear stress (τ) values at each stress state, to obtain the relevant parameters a and α from which c and ϕ can be calculated, by using Equations 5.7 to 5.9.

The cohesion (c) and internal friction angle (ϕ) calculated by the indirect method for the ferricrete material tested were 308 kPa and 50.9° respectively for all the saturation and relative densities within the stress conditions tested. These values are dependant on the parent material, and because the ferricrete tested was of high quality, the values for other types of materials are expected to be lower.

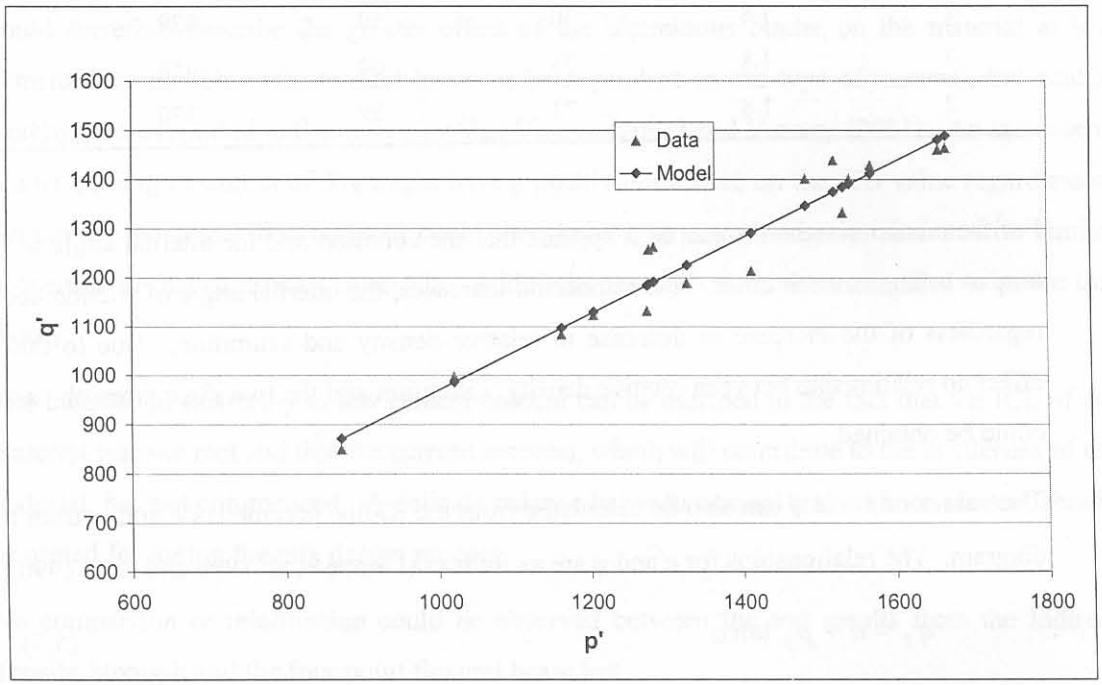

Figure 5.15 $p_f - q_f$ diagram from static triaxial tests

5.5 LABORATORY ELASTIC MODULUS (M_R)

The dynamic triaxial test results were used to calculate the elastic or resilient stiffness of the materials. Specimens were prepared for each material at two compaction levels and two degrees of saturation. The tests were performed at stress ratios of 0.20, 0.55 and 0.9 with confining pressures of 80 and 140 kPa for each stress ratio.

The stress ratio of a material is the ratio between the applied stress and die maximum shear strength at the failure envelope of the material. Theyse (2000) derived Equation 5.10 for the calculation of the stress ratio. It is graphically presented in Figure 5.16.

$$SR = \frac{\sigma_1^a - \sigma_3}{\sigma_1^m - \sigma_3} = \frac{\sigma_1^a - \sigma_3}{\sigma_3\left[\tan^2\left(45° + \frac{\phi}{2}\right) - 1\right] + 2.c.\tan\left(45° + \frac{\phi}{2}\right)} \quad (5.10)$$

where: SR = Stress ratio

σ_3 = minor principal stress or confining pressure (kPa)

c = cohesion (kPa)

ϕ = internal angle of friction (degrees)

σ_1^a = working or applied major principal stress (kPa)

σ_1^m = maximum allowable major principal stress for given ϕ, c, and σ_3 (kPa)

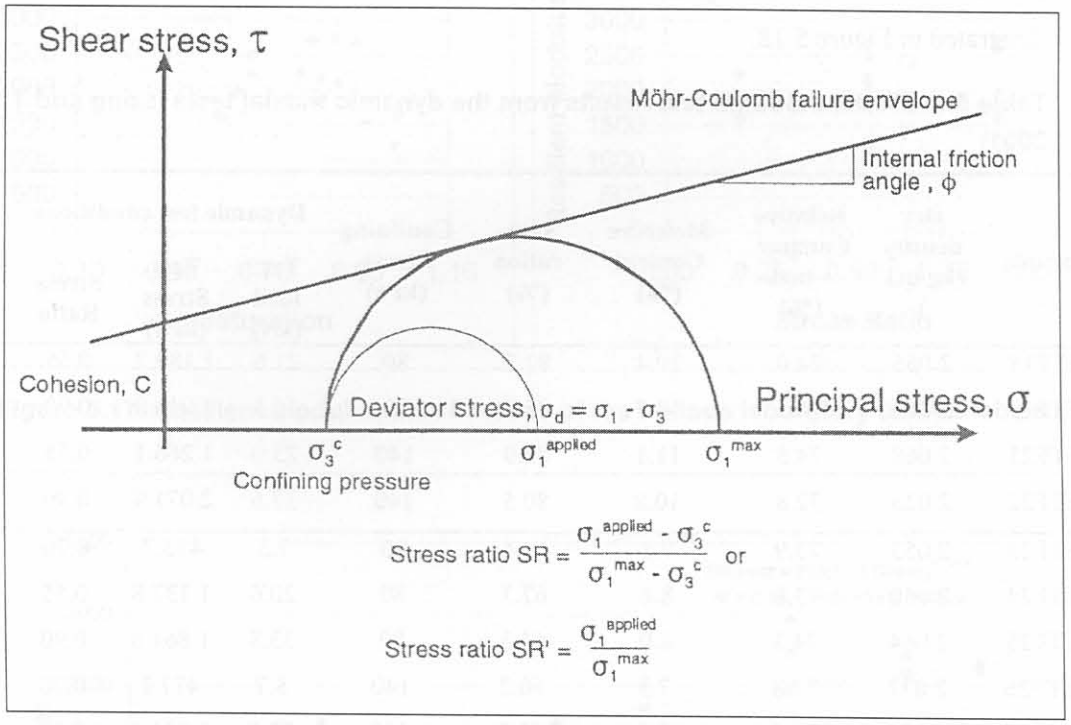

Figure 5.16 Möhr stress circles representation of the stress ratio concept (Theyse: 2000)

The complete results of the dynamic triaxial tests were documented in detail by Long and Theyse (2001).

A summary of the elastic modulus results from the dynamic triaxial tests on the emulsion treated ferricrete are presented in Table 5.8. The tests were done with 2.0 % cement and 1.8% net bitumen.

The elastic modulus ranged between 1 200 MPa and 2 700 MPa with an average of 2 039 MPa, a standard deviation of 450 MPa and a coefficient of variation of 22 %.

The resilient modulus as determined by the dynamic triaxial test is essentially a compressive elastic modulus. The values give an indication of the compressive behaviour of the material and do not necessarily describe the flexibility, tensile, or permanent deformation response of the material. It is however assumed that the flexibility, tensile and permanent deformation behaviour will be similar.

Figure 5.17 presents the influence of different parameters on the resilient modulus.

The only parameter that demonstrated some influence on the resilient modulus was the stress ratio. The confining pressure, relative density and degree of saturation produced a large amount of scatter and no definite relationship could be observed.

The bulk stress (Θ) can be calculated from the applied stress ratio and confining pressure. A plot with the bulk stress against the resilient modulus revealed some stress dependency as illustrated in Figure 5.18.

Table 5.8 Elastic modulus test results from the dynamic triaxial tests (Long and Theyse: 2001)

Sample	Dry density (kg/m3)	Relative Compac - tion (%)	Moisture Content (%)	Satu- ration (%)	Confining Stress (kPa)	Dynamic test conditions			Elastic Modulus (MPa)
						Test load (kN)	Test Stress (kPa)	Stress Ratio	
ETF18	2 055	74.0	10.4	82.2	80	21.6	1 189.7	0.55	2 160
ETF19	2 062	74.3	10.7	85.7	80	35.3	1 946.8	0.90	2 721
ETF21	2 068	74.5	11.1	89.9	140	23.0	1 266.1	0.55	2 657
ETF22	2 023	72.8	10.8	80.5	140	37.6	2 071.9	0.90	2 712
ETF23	2 053	73.9	7.8	61.4	80	7.5	413.7	0.20	1 607
ETF24	2 050	73.8	8.6	67.3	80	20.6	1 137.8	0.55	2 224
ETF25	2 064	74.3	8.0	64.3	80	33.8	1 861.8	0.90	1 964
ETF26	2 077	74.8	7.3	60.2	140	8.7	477.1	0.20	1 615
ETF27	2 070	74.5	8.3	67.5	140	23.8	1 311.9	0.55	2 507
ETF28	2 088	75.2	7.3	61.4	140	39.0	2 146.8	0.90	2 594
ETF29	2 164	77.9	9.4	92.2	80	10.4	575.6	0.20	1 530
ETF30	2 181	78.5	8.1	82.3	80	28.7	1 582.9	0.55	1 857
ETF31	2 143	77.2	10.5	98.6	80	47.0	2 590.2	0.90	1 615
ETF32	2 114	76.1	11.2	99.2	140	11.7	646.4	0.20	1 662
ETF33	2 104	75.8	11.3	98.1	140	32.3	1 777.6	0.55	1 223
ETF35	2 150	77.4	8.2	78.1	80	11.1	610.0	0.20	2 249
ETF36	2 152	77.5	9.0	86.1	80	30.4	1 677.5	0.55	2 102
ETF38	2 148	77.3	8.5	80.6	140	13.0	717.4	0.20	1 830
ETF39	2 152	77.5	7.9	75.5	140	35.8	1 972.9	0.55	1 970

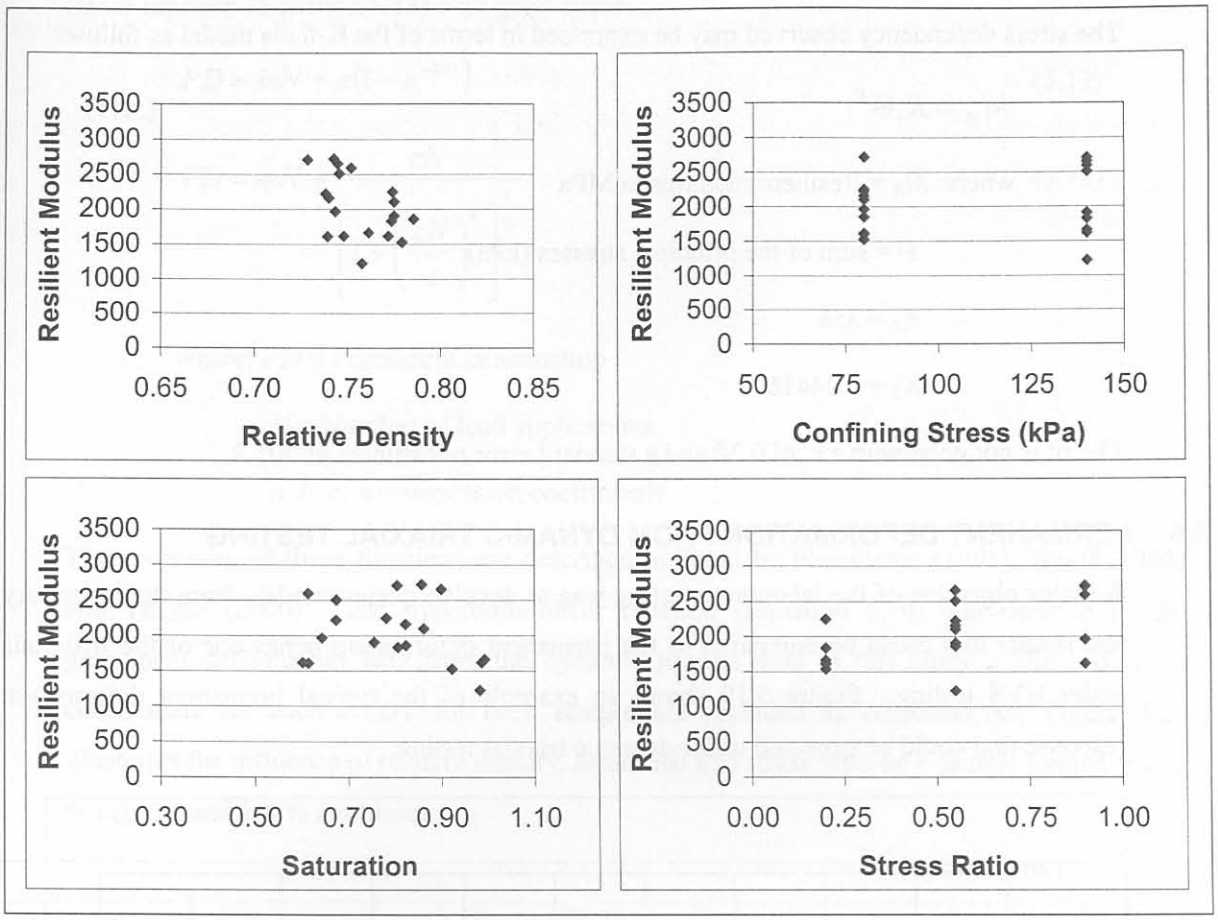

Figure 5.17 Resilient modulus as a function of the various laboratory test variables

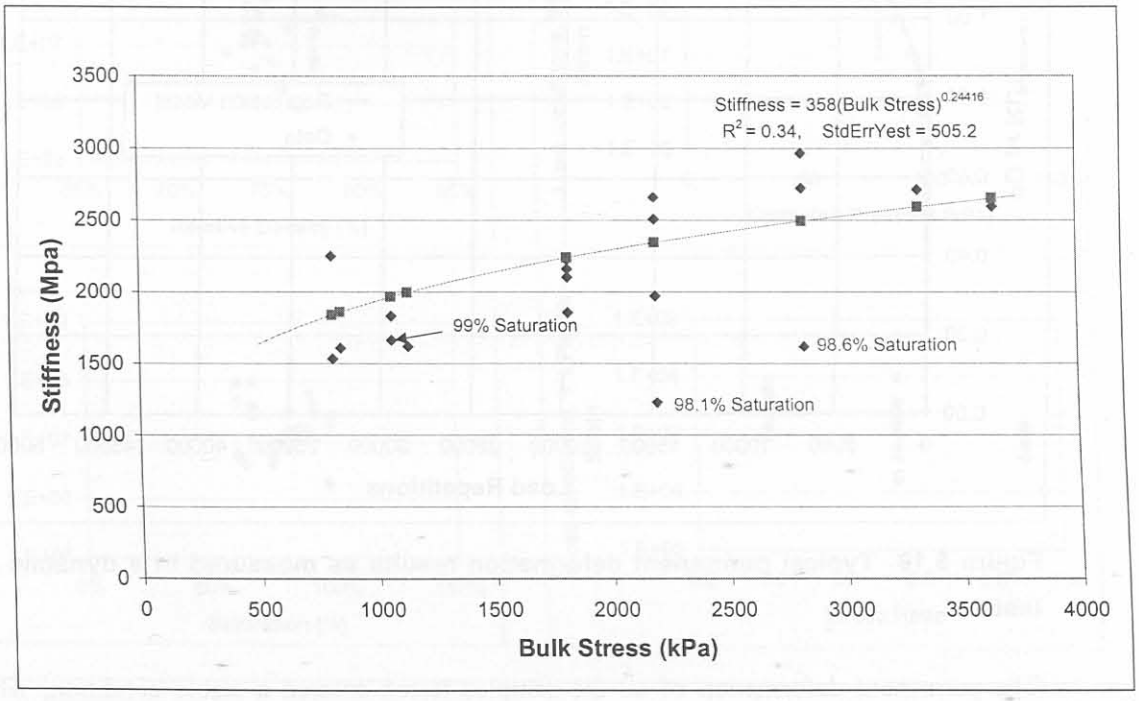

Figure 5.18 Resilient modulus vs. Bulk stress

The stress dependency observed may be expressed in terms of the K-theta model as follows:

$$M_R = K_1 \Theta^{K_2} \tag{5.11}$$

where: M_R = Resilient modulus in MPa

Θ = sum of the principal stresses (kPa)

$K_1 = 358$

$K_2 = 0.24416$

The fit is not good with a r^2 of 0.34 and a standard error of estimate of 505.2.

5.6 PERMANENT DEFORMATION FROM DYNAMIC TRIAXIAL TESTING

A major objective of the laboratory testing was to develop design models from the laboratory test results that could be compared to the permanent deformation behaviour of the materials under HVS testing. Figure 5.19 shows an example of the typical permanent deformation response that could be expected under dynamic triaxial testing.

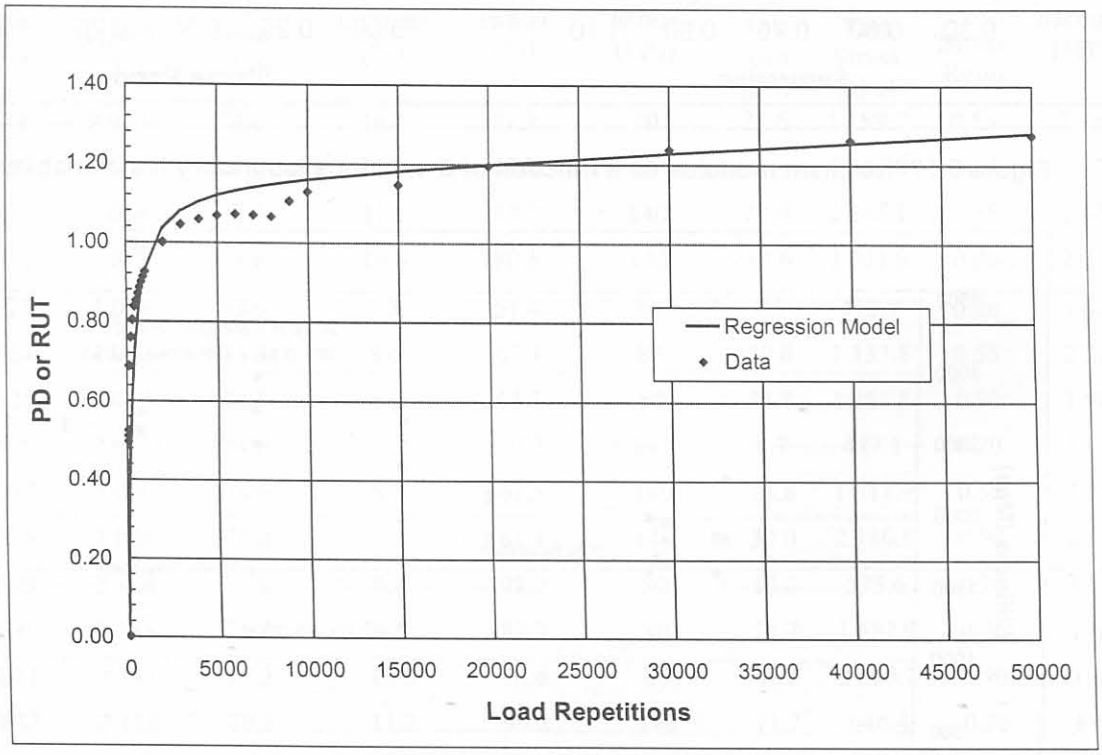

Figure 5.19 Typical permanent deformation results as measured in a dynamic triaxial test

The permanent deformation of all the samples tested entered a stable condition, where the permanent deformation increased linearly with increasing cycles. The permanent deformation

data can be fitted with either the exponential-linear function (Equation 5.12) or the hyperbolic-linear function (Equation 5.13) with good success.

$$PD = mN + a\left(1 - e^{-bN}\right) \tag{5.12}$$

$$PD = mN + \frac{cN}{\left[1 + \left(\frac{cN}{a}\right)^{b}\right]^{\frac{1}{b}}} \tag{5.13}$$

where: PD = Permanent deformation

N = Number of load applications

a, b, c, n = regression coefficients

The properties of these functions are described in detail by Shackleton (1995), Wolff (1992) and Theyse (2000). The hyperbolic-linear function (Equation 5.10) was used to fit the permanent deformation data from the dynamic triaxial tests in this study. The regression coefficients for each LVDT for each sample are included as Appendix A. Figure 5.20 illustrates the influence of relative density, saturation and stress ratio on a sample treated with 2 % cement and 1.8 % net bitumen.

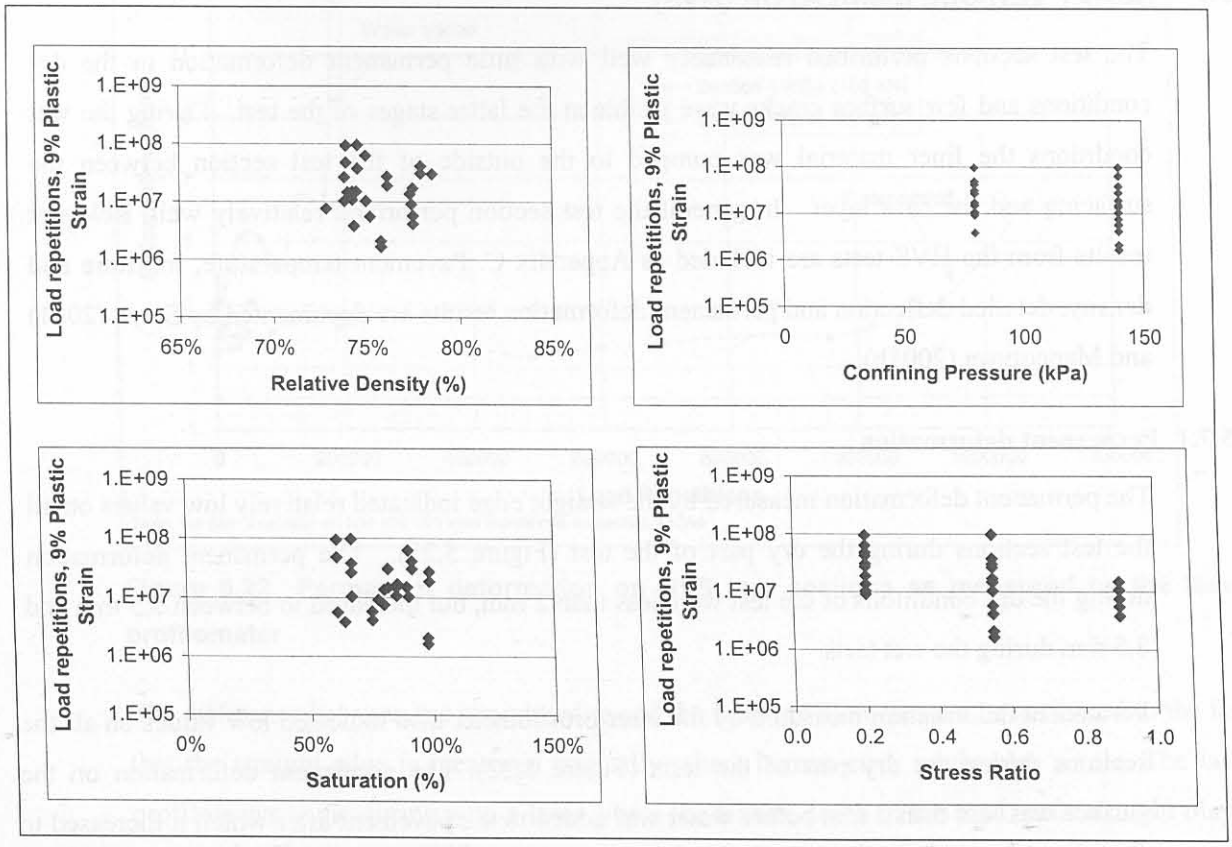

Figure 5.20 Influence of Relative Density, degree of saturation and stress ratio on the number of repetitions to 9 % plastic strain

The number of load repetitions is largely insensitive to the relative density and degree of saturation when bitumen emulsion is added to the sample. The results for an untreated ferricrete, as documented by Long and Theyse (2001), shows a sensitivity towards relative density and degree of saturation for untreated samples. The stress ratio however seems to have some influence on the number of load repetitions to 9% plastic strain, although a large amount of scatter is present. Long and Theyse (2001) developed the following statistical relationship between the various parameters in which only the plastic strain (*PS*) and strain ratio (*SR*) are statistically significant:

$$\log N = 4.78 + 0.07PS - 0.68SR \qquad (r^2 = 0.30) \qquad (5.14)$$

where: N = Number of load repetitions

PS = Plastic strain (%)

SR = Stress ratio as defined in Equation 5.7

According to Long and Theyse (2001) there was no significant improvement in the permanent deformation resistance of the ferricrete by the addition of bitumen emulsion when compared to the untreated and cement treated samples as tested under dynamic triaxial tests.

5.7 HEAVY VEHICLE SIMULATOR (HVS)

The test sections performed reasonably well with little permanent deformation in the dry conditions and few surface cracks were visible at the latter stages of the test. During the wet conditions the finer material was pumped to the outside of the test section between the surfacing and the base layer. In general the test section performed relatively well. Relevant results from the HVS tests are included as Appendix C. Pavement temperature, moisture and density, detailed deflection and permanent deformation results are documented by Steyn (2001) and Mancotywa (2001b).

5.7.1 Permanent deformation

The permanent deformation measured by the straight edge indicated relatively low values on all the test sections during the dry part of the test (Figure 5.21). The permanent deformation during the dry conditions of the test were less than 2 mm, but increased to between 5.5 mm and 8.5 mm during the wet tests.

Permanent deformation measured by the laser profilometer also indicated low values on all the sections during the dry part of the tests (Figure 5.22). The permanent deformation on the surface was less than 2 mm before water was added to the pavement after which it increased to between 5 and 6 mm.

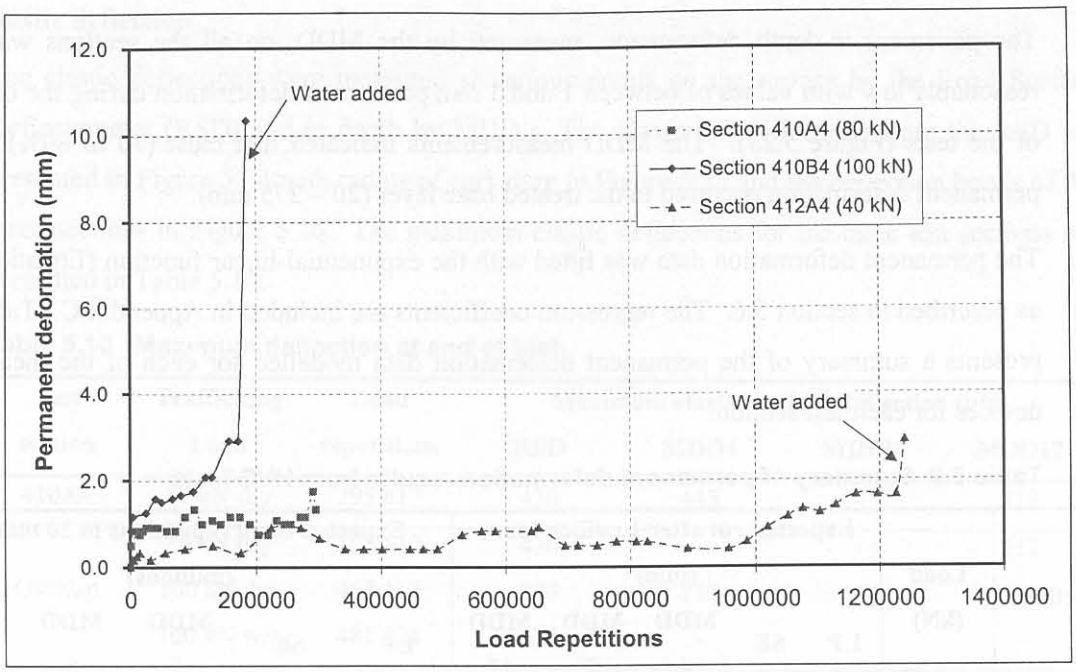

Figure 5.21 Permanent deformation on HVS test sections as measured by the straight edge

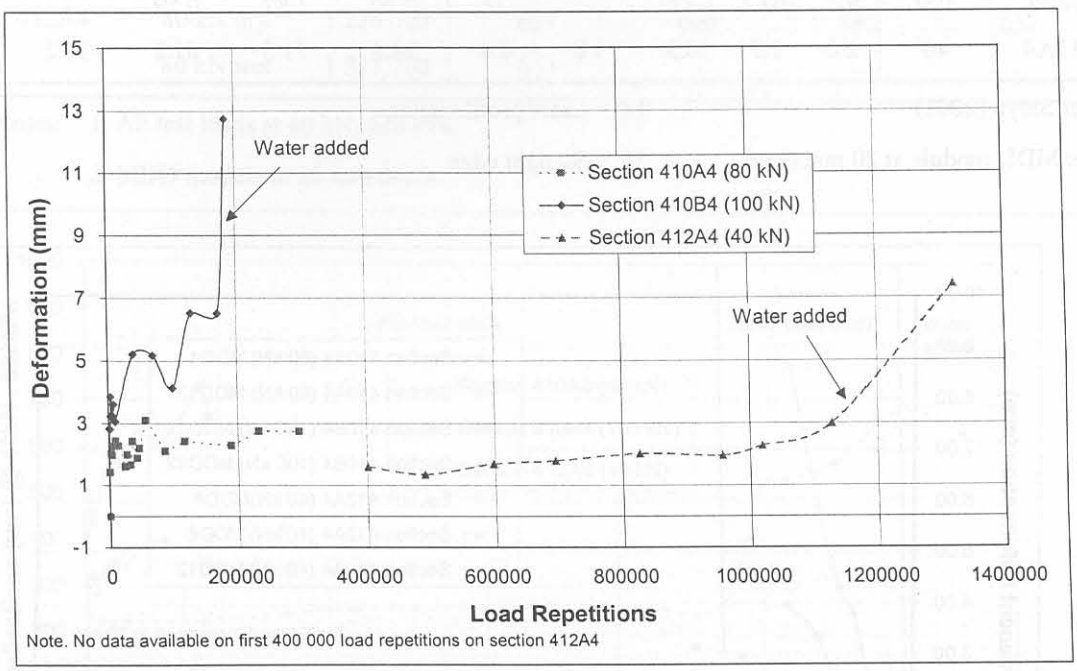

Figure 5.22 Permanent deformation on HVS test sections as measured by the laser profilometer

The difference between the straight edge and the laser profilometer can be attributed to the fact that the straight edge is measured manually where human error might play a role. The laser profilometer is measuring with a laser where the texture depth of the road surface might play a role.

The pavement in-depth deformation, measured by the MDD, on all the sections was also reasonably low with values of between 1 and 3 mm permanent deformation during the dry part of the tests (Figure 5.23). The MDD measurements indicated that most (70 to 80%) of the permanent deformation occurred in the treated base layer (20 – 275 mm).

The permanent deformation data was fitted with the exponential-linear function (Equation 5.9) as described in section 5.6. The regression coefficients are included in Appendix C. Table 5.9 presents a summary of the permanent deformation data modelled for each of the measuring devices for each test section.

Table 5.9 Summary of permanent deformation results from HVS tests

Section	Load (kN)	Expected rut after 1 million loads (mm)					Expected Load repetitions to 20 mm rut (millions)				
		LP	SE	MDD 4	MDD 8	MDD 12	LP	SE	MDD 4	MDD 8	MDD 12
410A4*	80	11.1	2.2	8.9	-	7.8	1.80	9.09	1.12	-	1.28
Overlap*	80/100	3.3	10.2	-	-	-	6.06	1.96	-	-	-
410B4*	100	9.1	10.7	17	-	32	2.20	1.87	0.59	-	0.31
412A4	40	2.0	1.7	0.3	1.8	0.4	24.8	71.5	61.2	33.2	50.7

*After Steyn (2001) LP = Laser profilometer

Note: MDD module at 20 mm depth SE = Straight edge

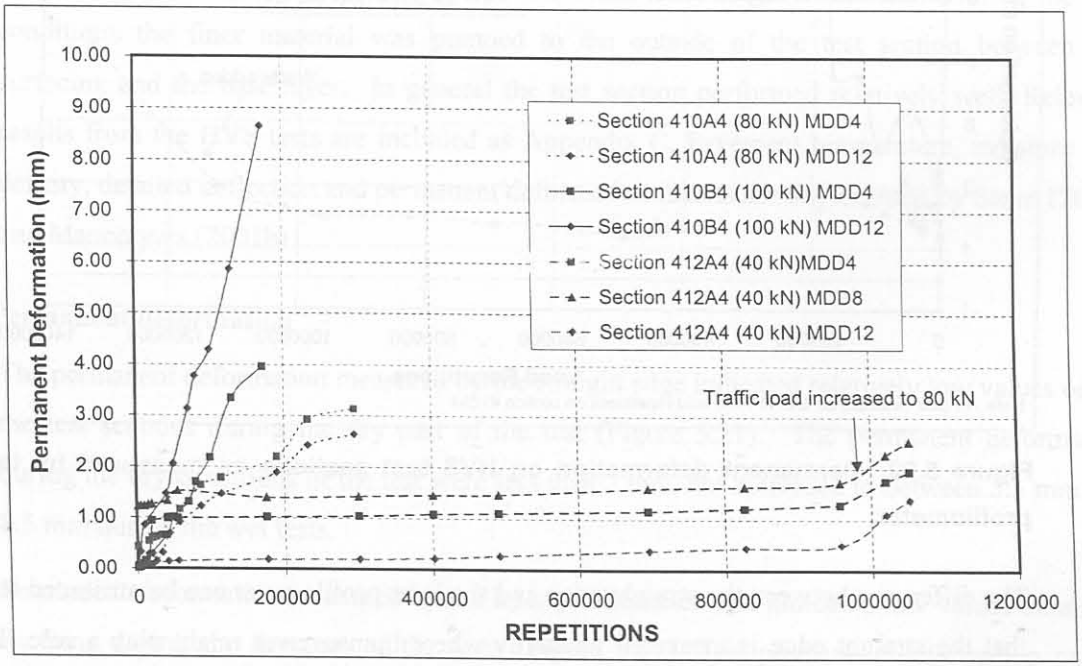

Figure 5.23 Permanent deformation on HVS test sections as measured by the MDD module at 40 mm.

5.7.2 Elastic deflection

The elastic deflections were measured at various points on the surface by the Road Surface Deflectometer (RSD) and in depth by MDD's. The maximum deflections from the RSD are presented in Figure 5.24 with radius of curvature in Figure 5.25 and the deflection bowls of the three sections in Figure 5.26. The maximum elastic deflections for the three test sections are presented in Table 5.10.

Table 5.10 Maximum deflection at end of test

Test section	Trafficking Load	Load repetitions	Maximum elastic surface deflection (μm)			
			RSD	MDD4	MDD8	MDD12
410A4	80 kN dry	295 617	430	443	-	517
Overlap	80 kN dry	295 617	430	-	-	517
	100 kN dry	467 117	728	717	-	-
	100 kN wet	481 024	678	-	-	-
410B4	100 kN dry	171 500	778	-	-	848
	100 kN wet	185 407	646	-	-	-
412A4	40 kN dry	957 121	268	281	311	237
	80 kN dry	1 226 000	687	660	680	637
	80 kN wet	1 321 700	637	-	-	-

Notes: 1. All test loads at 40 kN, 620 kPa

2. MDD module at 20 mm depth

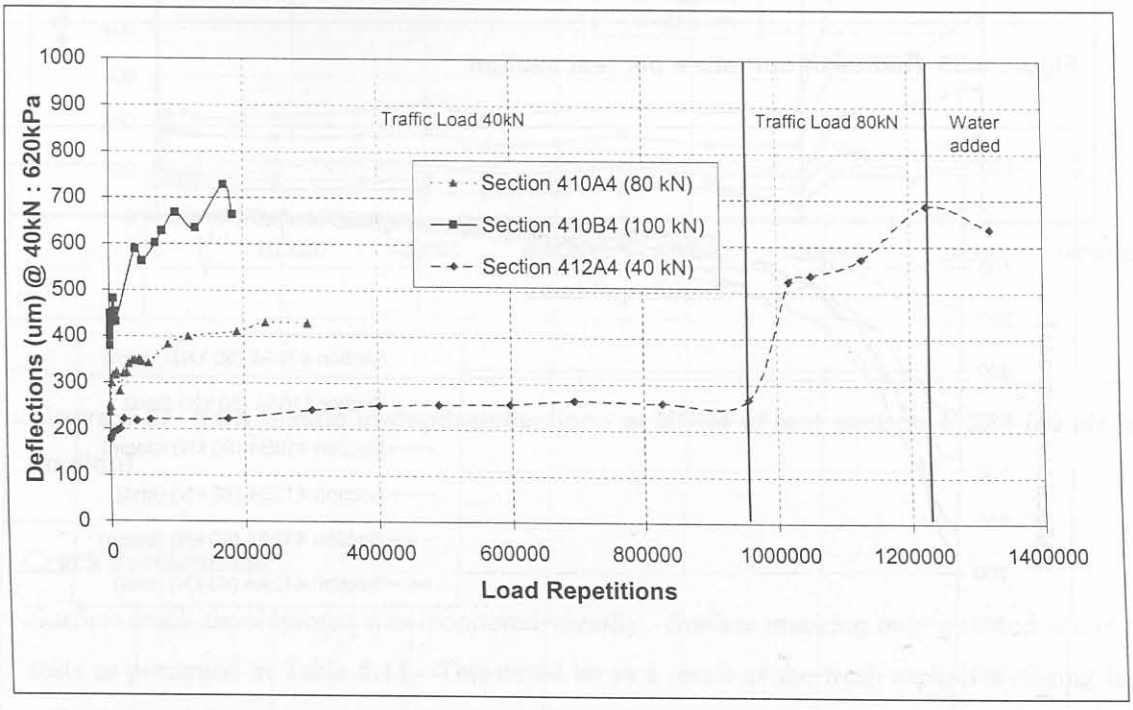

Figure 5.24 Maximum RSD elastic deflection per test section

For the 80 kN and 100 kN tests, the maximum deflection increased sharply during the test and when the tests were terminated the maximum deflections were almost twice their original value. For the 40 kN test, the maximum deflection did not show an increase during the duration of the 40 kN test. It increased sharply when the trafficking load was increased to 80 kN and terminated at values similar to that of the 100 kN test. This indicates that the pavement is sensitive to overloading.

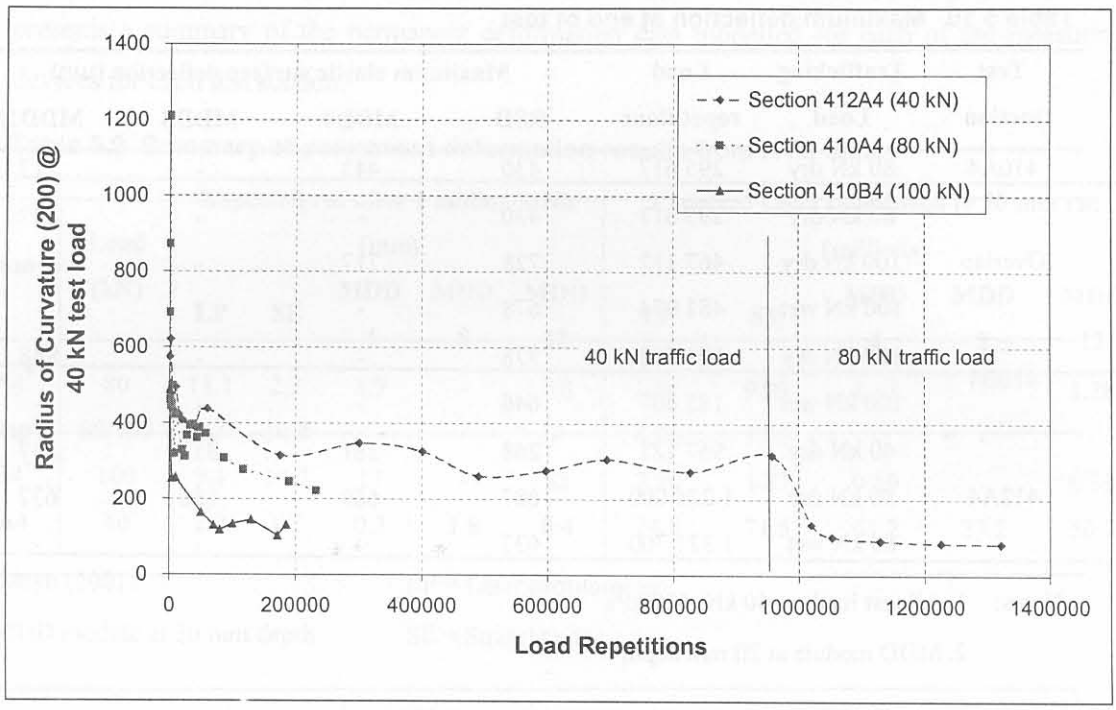

Figure 5.25 Radius of curvature per test section

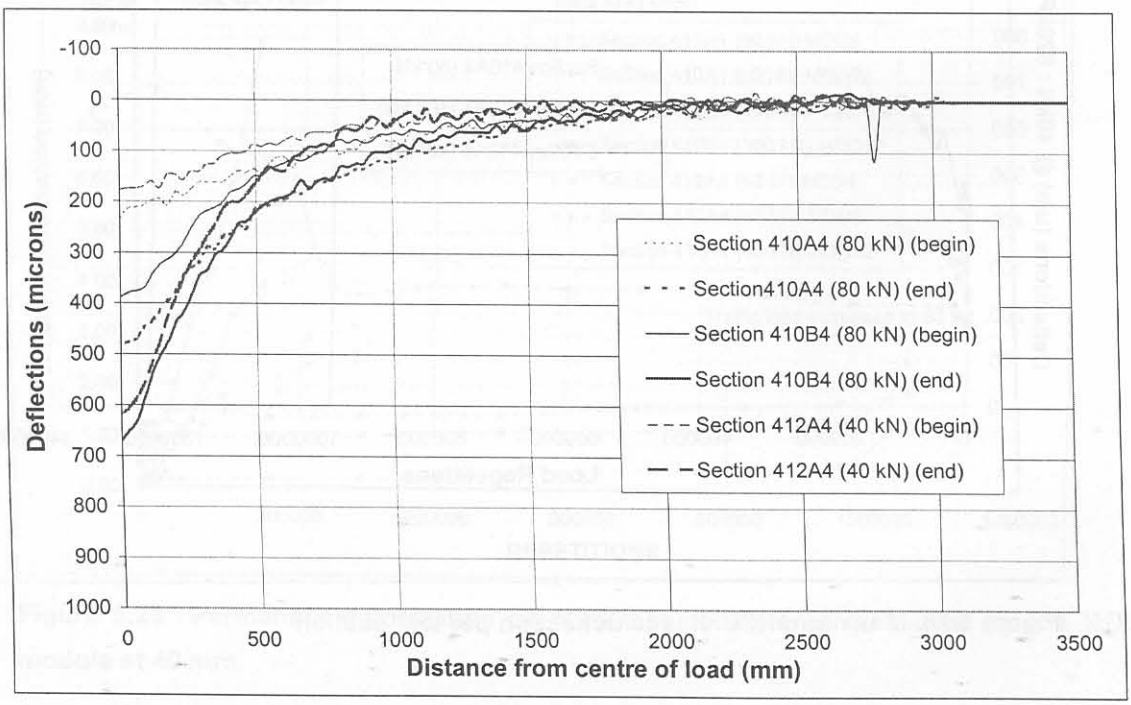

Figure 5.26 Deflection bowls per test section

The deflection bowls from the RSD data indicated the influence of an increasing wheel load on the maximum deflection and shape of the deflection bowl. The shape of the deflection bowls and the radius of curvature (*ROC*) showed that there was a change in the elastic behaviour of the pavement structure during trafficking. This change in elastic behaviour is not as distinct as in the case with cement treated layers, and it appears that layers treated with emulsion change their elastic behaviour more gradually during trafficking. The *ROC* also decreases when the trafficking wheel load is increased which indicates that the pavement structure tends to reduce its load spreading capability in the upper layers.

Figure 5.27 shows the elastic in-depth deflections at MDD 4 of section 412A4 (40 kN test section). This data indicated that the elastic in-depth deflections were equally distributed between the layers shallower than 650 mm. It also appears that the material reacted in a linear elastic fashion, as the increased elastic deflection measured is similar to the increased test wheel load (Figure 5.28).

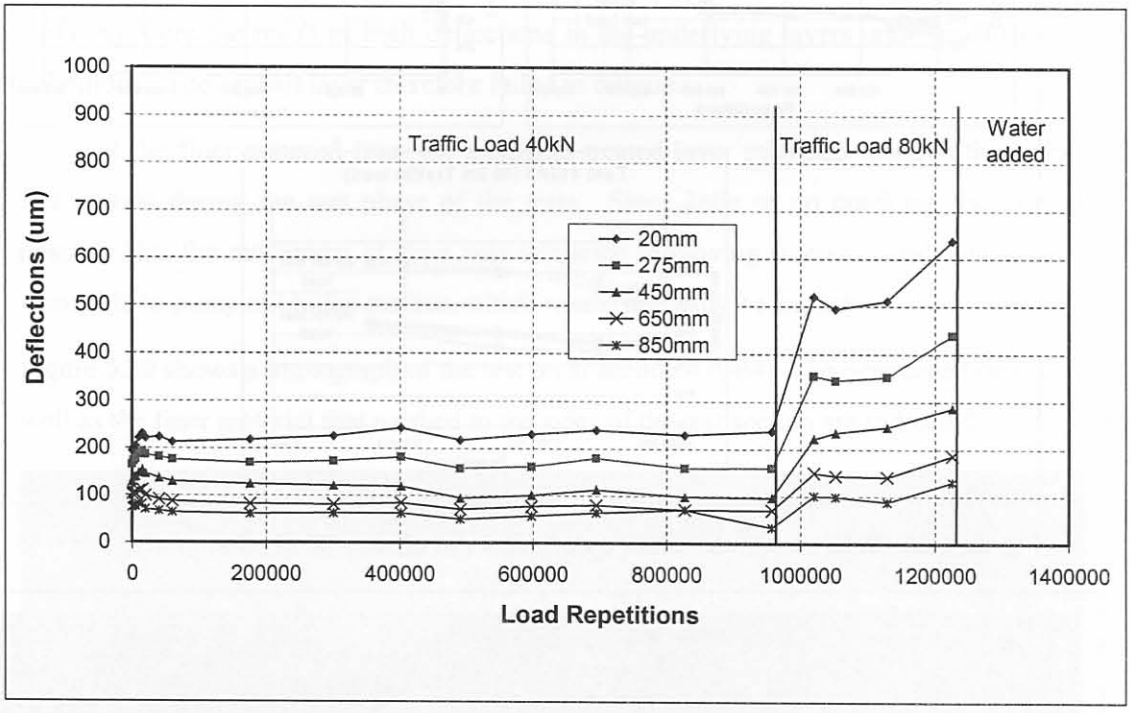

Figure 5.27 MDD elastic in-depth deflections at MDD4 of test section 412A4 (40 kN test section)

5.7.3 Crack development

Surface crack development was monitored visually. Surface cracking only initiated late in the tests as presented in Table 5.11. This could be as a result of the fresh asphalt surfacing layer over the emulsion treated base layer.

The crack development for sections 410B4 and 412A4 are shown in Figure 5.29. The figures show the final crack patterns of the test sections. A detailed record of the crack patterns for all the test sections is included in Appendix C.

Table 5.11 Crack development on HVS test sections

Test section	Number of repetitions before surface cracking was detected
410A4	No cracking developed before test was terminated at 295 617
410B4	129 544
412A4	1 226 000*

* First 957 121 repetitions were at 40 kN and the last 268 879 at 80 kN

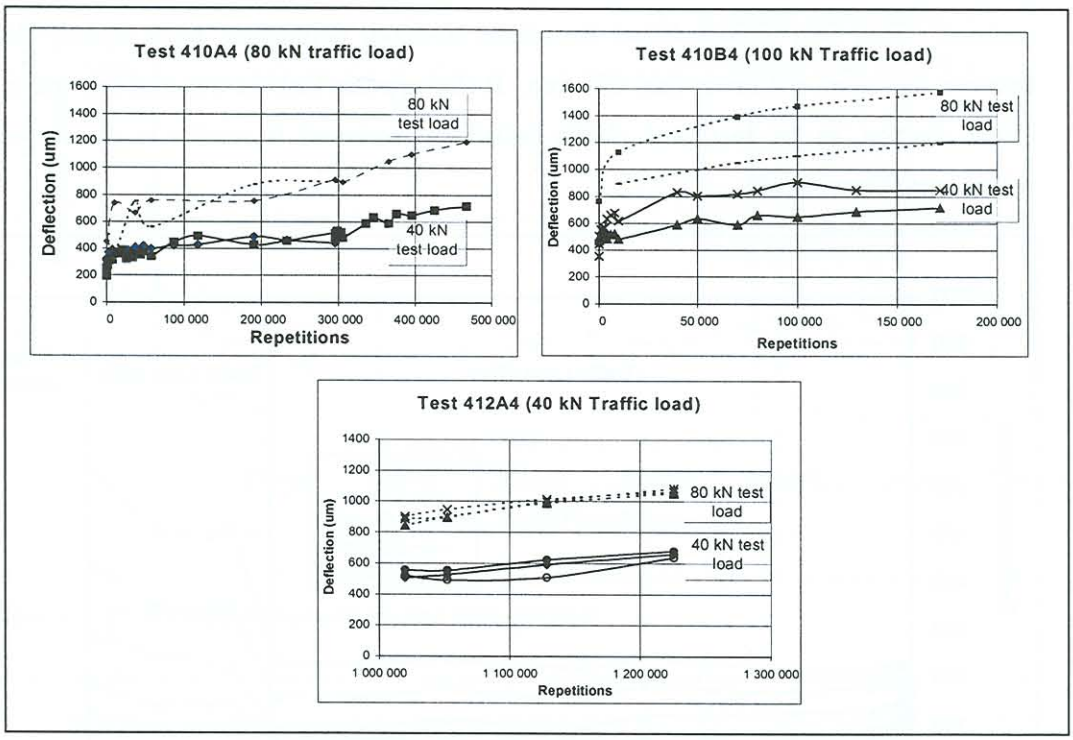

Figure 5.28 MDD maximum elastic deflection at 40 and 80 kN test loads

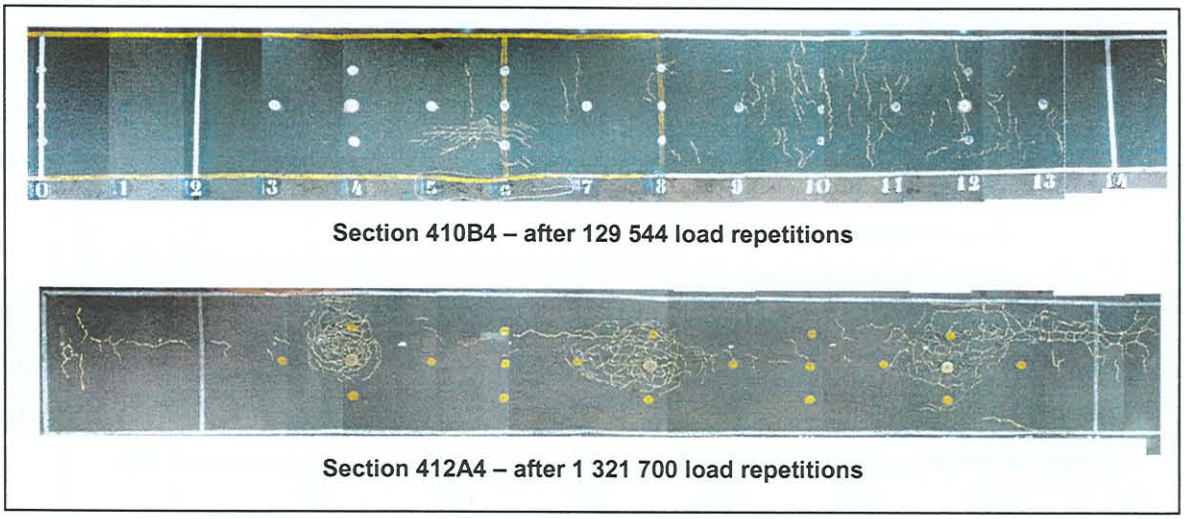

Figure 5.29 Final crack patterns

5.7.4 Test pits

Test pits were opened at the test sections as described by Steyn (2001) and Mancotywa (2001b). The objective of the test pits was to observe the behaviour and condition of the various layers after trafficking. On sections 410A4 and 410B4 the first test pit was opened to a depth of 600 mm, the second only through the base layer (300 mm) and for the third only the surfacing was removed. On section 412A4 only one test pit to a depth of 800 mm was opened.

The emulsion treated layer broke down into large lumps during the 80 and 100 kN tests (sections 410A4 an 410B4) but no indication of this could be found during the 40 kN test (section 412A4).

On the 40 kN test, no cracks in the emulsion treated layer could be observed to the full depth profile of the test pit. The cracks that reflected on the surface of the road were only in the asphalt layer and none of these cracks could be followed into the emulsion treated layer. As most of the cracking started during the wet period of the tests, the cracks in the asphalt surfacing were the result of high deflections in the underlying layers under trafficking in wet conditions. The asphalt layer therefore failed in fatigue.

Some of the finer material from the emulsion treated layer migrated towards the sides of the test section during the wet phase of the tests. Since little or no cracking was present it is possible that the movement of fines was restricted to moving sideways and very few of them were able to pump out to the surface, which would normally be expected.

Figure 5.30 shows a photograph of the test pit at section 410B4. The permanent deformation as well as the finer material that washed to the sides of the test section are indicated on the photo.

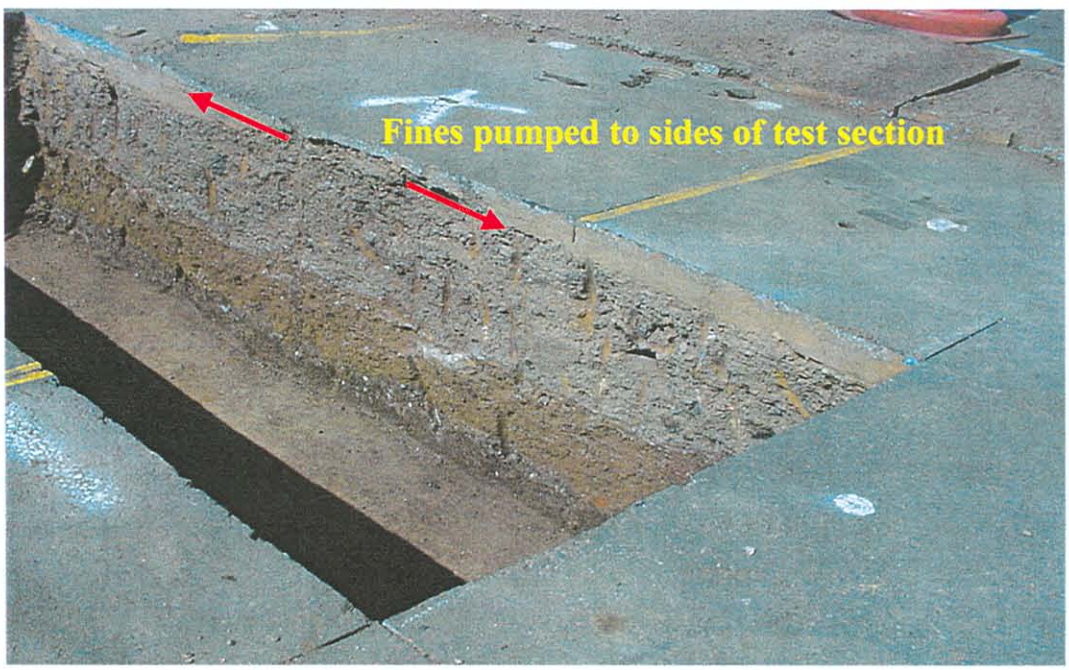

Figure 5.30 Test pit at section 410B4

5.7.5 Effective elastic stiffness

The depth deflection profiles were used to back-calculate the effective elastic moduli (E – moduli) for the different layers at various stages of trafficking. The subgrade was assumed to be of infinite depth i.e. an elastic half space. The dual wheels were spaced at 350 mm and the effective moduli were calculated directly under one of the wheels. It was found that more realistic E moduli were obtained from this approach because the linear elastic theory calculate unrealistically low moduli for the base layer if calculated between the wheels. These results compared favourably with the method used by de Beer (1989) where the wheel spacing was reduced to ensure that the contact areas met. A Poisson's ratio of 0.35 was used in the backcalculation and an analysis at different Poisson's ratios indicated that the stiffness was not sensitive to small variations. This was also found by Fossberg (1970) and Otte (1972) on cement stabilised base layer materials. Work by Semmelink (2001) and Semmelink et al (2000b), however, indicated values for the Poisson's ratio of the emulsion treated ferricrete as low as 0.1.

The results show that the E moduli of the emulsion treated base layer decreases gradually with trafficking. For higher wheel loads this reduction is more rapid than for lower wheel loads. It is believed that this reduction in E moduli, together with the change in the shape of the deflection bowl, as discussed in section 5.7.2, will enhance the understanding of the behaviour of emulsion treated layers.

Concepts of the reduction in E moduli for cement treated layers were introduced into South Africa as early as 1978 (Otte: 1978). Freeme (1983) proposed the concept of "effective stiffness or moduli" which states that a bound (bituminous or cementitious) layer cracks in fatigue or breaks down, then the layer ceases to behave as a homogeneous continuum in the way normally assumed in theoretical analysis. The concept of pre-cracked and post-cracked phases was introduced by Freeme (1983) and is illustrated in Figure 5.31.

Research by de Beer and Grobler (1993), Mancotywa (2001a) as well as results from this study indicated a similar reduction of E moduli in emulsion treated layers.

The effective E moduli on the 40 and 80 kN started at between 1 500 and 2 700 MPa while the E moduli on the 100 kN section started at 1 000 MPa. Table 5.12 and Figure 5.32 present the backcalculated E moduli for the three test sections at the beginning and end of each test.

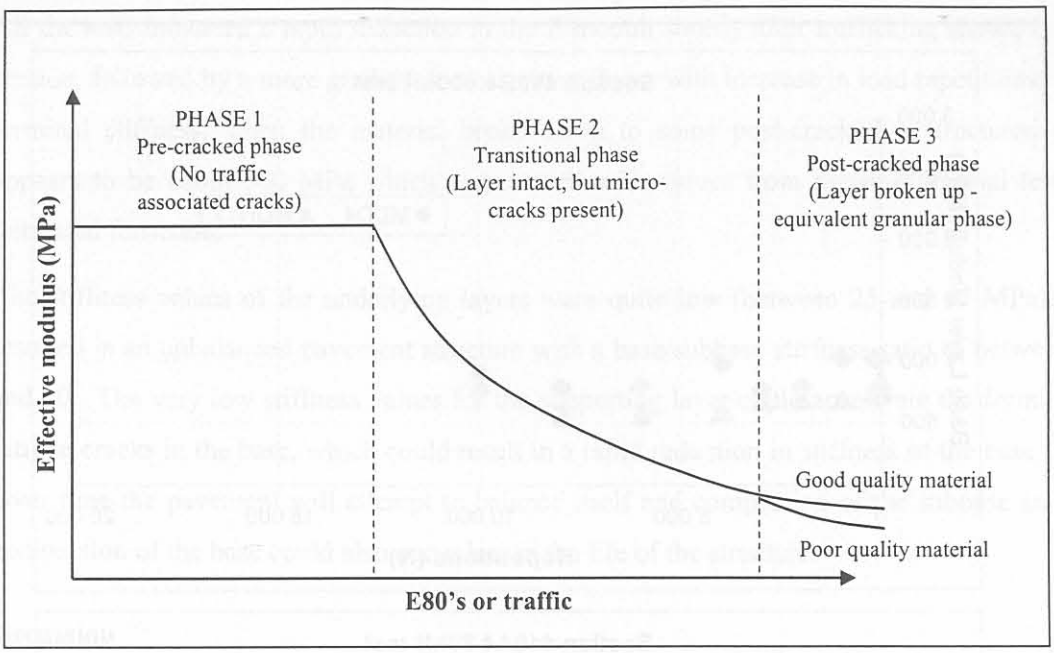

Figure 5.31 Reduction of E-moduli of C3 material under trafficking (Freeme: 1983)

Table 5.12 Summary of backcalculated E moduli for HVS test sections.

Section	Trafficking load	Initial Stiffness (MPa)	Final stiffness (MPa)	Number of repetitions
410A4	80 kN	2 000 – 2 700	1 100	295 617
Overlap	80 kN	2 000 – 2 700	1 000	295 617
	100 kN	1 000	850	467 117
410B4	100 kN	1 000	750	171 500
412A4	40 kN	1 750 – 2 250	750 – 1 250	957 121
	80 kN		350 – 500	1 226 000

All the tests commenced at an initial effective E modulus of between 1 750 and 2 700 MPa which agree well with the dynamic triaxial test results. The 100 kN test, however, started at a stiffness of 1 000 MPa. It is assumed that the 100 kN trafficking load caused the reduction in E modulus from the start of the test and could also be the reason for the scatter in the data and for the E modulus not to decrease with increase in load repetitions (Figure 5.32b). This was also the case at MDD4 in the 80 kN test (Figure 5.32a). The reduction of E moduli with increase in load repetitions was clearly evident on the 40 kN test as can be seen in Figure 5.32c. The stiffness after 957 121 repetitions at 40 kN was in the range of between 750 and 1 250 MPa and reduced further when the wheel load was increased to 80 kN to a value of around 500 MPa. Dynamic triaxial tests done on the untreated ferricrete indicated that the average resilient modulus of the untreated ferricrete was about 660 MPa. This relatively high value for natural gravel can be attributed to the well-graded material obtained from the deep in situ recycling.

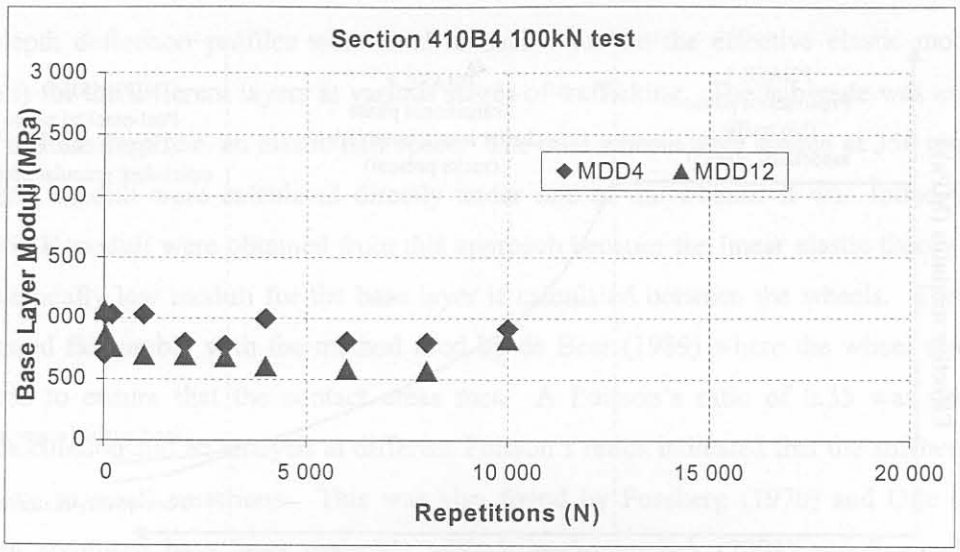

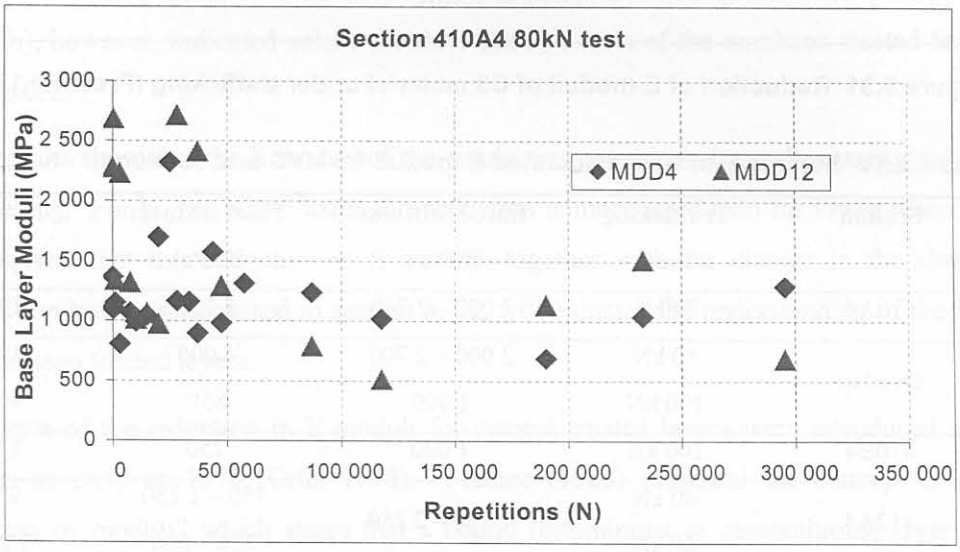

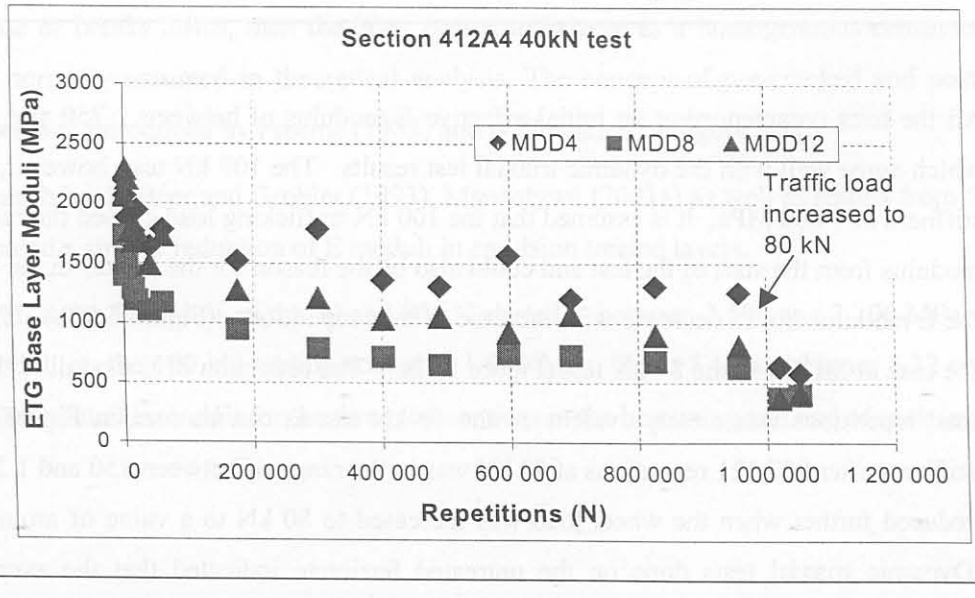

Figure 5.32 Back calculated E moduli for the different test sections

All the tests indicated a rapid reduction in the E moduli shortly after trafficking started on the section, followed by a more gradual decrease in stiffness with increase in load repetitions. The terminal stiffness, when the material broke down to some post-cracked or fractured state appears to be about 500 MPa which agrees well with values from dynamic triaxial tests of untreated ferricrete.

The stiffness values of the underlying layers were quite low (between 25 and 45 MPa), and resulted in an unbalanced pavement structure with a base/subbase stiffness ratio of between 11 and 20. The very low stiffness values for the supporting layer could accelerate the forming of fatigue cracks in the base, which could result in a rapid reduction in stiffness of the base layer. Over time the pavement will attempt to balance itself and compaction of the subbase and de-compaction of the base could also occur late in the life of the structure.

5.7.6 Discussion

The emulsion treated test sections performed well during the HVS tests. The thickness of the treated recycled layer (250 mm) could have contributed to this performance of the pavement. Very little permanent deformation was measured at the surface, throughout the dry phases of the tests, with crack development mainly restricted to the wet tests. Although most of the permanent deformation occurred within the emulsion treated layer, the amount of permanent deformation was small. The small contribution of the lower layers to the permanent deformation as well as the elastic deflection, indicate that the emulsion treated layer provided good protection for the subgrade and other lower lying layers.

The reduction in the E moduli and gradual change in the deflection bowl, confirm that the behaviour of emulsion treated layers are a phased behaviour. The test pits however revealed that the second phase might not necessarily be a so called "equivalent granular" phase, but rather a phase with a reduced stiffness in which the permanent deformation of the layer (as a base layer) might be the dominant failure mechanism. The mechanism of the permanent deformation could be similar to that present in unbound granular base layers, which is a combination of gradual shear failure and densification or compaction during the initial bedding in phase.

5.8 CONCLUSIONS

The following conclusions could be drawn from the laboratory and HVS test results included in this study:

- The Initial Consumption of Lime (ICL) requires to be satisfied to enable the cement to add significant strength to the mix. Bitumen emulsion alone does not necessarily add strength to the material when the net bitumen content is less than 3 %.

- The cement contributes to the brittleness of the material while the bitumen emulsion contributes to the flexibility of the mix. The quantities of cement and net bitumen in the mix tend to cause the behaviour of the material to be more like a lightly cemented material than an asphalt material.
- There exists a fine balance between the cement and emulsion content in the mix to ensure the optimal strength and flexibility that would be required in the structural design.
- The compaction method, compaction moisture and curing method applied to the laboratory samples may influence the results from the different laboratory tests. This experiment attempted to simulate field conditions as closely as possible by 28 day curing at ambient temperature.
- The static compressive shear strength parameters (c and ϕ) were estimated for the material in this study at 308 kPa and 50.9°, respectively.
- The initial resilient modulus of the emulsion treated material from both the laboratory testing and backcalculation from HVS in depth elastic deflections, was in the order of 2 000 MPa. The good grading of the material from the deep in-situ recycler may have contributed to the relative high stiffness value.
- The material has a stress sensitivity in the sense that the stiffness increases slightly with an increase in the bulk stress or stress condition within the material.
- The laboratory tests indicated that the permanent deformation of the untreated ferricrete was not significantly improved by the addition of emulsion and cement. The HVS, however, resulted in very low permanent deformation results, even after a high number of load repetitions.
- There is a definite phased behaviour in the elastic response of the material, although it was not as drastic as was the case with cement treated material. There seems to be a more gradual change in the elastic response as opposed to a rapid change at some stage during the life of the material.
- The HVS section showed very little cracking and most of the cracking was initiated only after the wet testing commenced. Most of the cracking appears to be limited to the asphalt surfacing of the pavement rather than in the emulsion treated layer.
- During the wet test, fine material was pumped to the sides of the test section, outside the trafficking section. Most of the fines were trapped between the base layer and the asphalt surfacing.

The behaviour of emulsion treated layers is at least a two phase behaviour with the first phase being a fatigue life phase with a high modulus of elasticity and a layer that would mainly fail in fatigue. Although no cracks were visible during the inspection of the test pits, it is reasonable

to believe that microcracks were present in the layer, which resulted in the reduced stiffness after a number of load applications. The second phase would be an "equivalent granular phase" with a reduced stiffness. This "equivalent granular phase" does not mean that the material is truly an unbound material in the complete sense, but rather that the stiffness properties of the material are similar to that of a granular material and that the failure mechanism of this phase would be permanent deformation due to gradual shear deformation.

5.9 RECOMMENDATIONS

The following recommendations are given regarding the structural design of emulsion treated layers:

- The initial stiffness or E moduli proposed for emulsion treated layers constructed by means of a *deep in-situ recycling machine* were 2 000 MPa, with the second phase (equivalent granular phase) stiffness of 500 MPa. It is important to note that these numbers referred to a parent material that is well graded and which fits the G6 material specification.
- The Poisson's ratio (μ) of the material, as used in the structural evaluation in both the fatigue life and post fatigue life phases, be 0.35. The use of this value is proposed until further formal research proves otherwise.
- The structural evaluation of an emulsion treated material be done as a two phase behaviour similar to that of cement treated material with a fatigue life phase as first phase and an "equivalent granular" phase as second phase.
- The strain at break (ε_b) should be obtained from four point flexural beam tests. The values from the results in this study approximate the values for cement treated materials, provided that the ICL is met. For estimation, the strain at break values assumed in Table 5.13, should be used. These values were averaged from the laboratory study for the possible different combinations of cement and emulsion contents and are valid for parent material of G5 to G7 quality. Special curing should be allowed for layers constructed without cement or at low cement contents below the ICL on parent materials of G4 to G7. This is however not recommended. The designer should keep in mind that the strain at break will reduce if more than the required amount of cement is added.

Table 5.13 Proposed values for strain at break for emulsion treated materials

		Net bitumen content	
		1% to 2 %	2% to 3.5%
Cement-content	Below ICL	325 με	500 με
	Slightly above ICL	145 με	230 με

- The compressive shear parameters should be obtained from static triaxial testing, but for estimation, values of 200 - 300 kPa for the cohesion (c) and 45° - 50° for the angle of internal friction (ϕ) can be assumed.

5.10 REFERENCES

Basson JEB, Wijnberger OJ and Skultety J, 1981, *The multi depth deflectometer: A multistage sensor for the measurements of resilient deflections and permanent deformations at various depths in road pavements*, Technical report RP/3/81, National Institute for Transport and Road Research, CSIR, Pretoria, South Africa.

Blabb R and Litzka J, 1995, *Measurements of the lateral distribution of heavy vehicles and its effects on the design of road pavements*, Proceedings of the Fourth International Symposium on Heavy Vehicles and Dimensions, edited by CB Winkler, University of Michigan Transportation Research Institute, Ann Arbor, United States, pp 389 – 395.

Das BM, 1990, *Principles of Geotechnical Engineering,* 2nd ed., PWS-KENT Publishing Company, Boston, United States.

De Beer M, Horak E and Visser AT, 1988, *The multi depth deflectometer (MDD) system for determining the effective elastic moduli of pavement layers*, First International Symposium on non-destructive testing of pavement and back calculation of moduli, ASTM STP 1026, Baltimore, United States.

De Beer M, 1989, *Aspects of the design and behaviour of road structures incorporating lightly cementitious layers*, PhD thesis, University of Pretoria, Pretoria, South Africa.

De Beer M and Grobler JE, 1993, *ETB's: Heavy Vehicle Simulator (HVS) evaluation of the heilbron sections*, Report RSC92/2/1, Division of Roads and Transport Technology, CSIR, Pretoria, South Africa.

Division of Roads and Transport Tevhnology (DRTT), 1987, *Accelerated testing; 1: The Heavy Vehicle Simulator*, Information Brochure, CSIR, Pretoria, South Africa.

Eades JL and Grim RE, 1964, *A quick test to determine the lime requirements for lime stabilisation*, Highway research Record no. 139, Washington DC, United States.

Fossberg PE, 1970, *Load-deformation characteristics of three layer pavements containing cement-stabilised bases*, PhD Thesis, University of Berkeley, California, United States.

Freeme CR. 1983, *Evaluation of pavement behaviour for major rehabilitation of roads*, Technical Report RP/19/83, National Institute for Transport and Road Research, CSIR, Pretoria, South Africa.

Lambe TW and Whitman RV, 1969, *Soil Mechanics*, Massachusetts Institute of Technology, John Wiley and Sons Inc., New York, United States

Long FM and Theyse HL, 2001, *Laboratory testing for the HVS Sections on Road P243-1*, Contract Report CR-2001/32, Transportek, CSIR, Pretoria, South Africa.

Mancotywa WS, 2000, *First level analysis report: Phase 1 HVS testing of experimental sections on road R2388 near Cullinan*, Contract Report CR-99/011, CSIR Transportek, Pretoria, South Africa, South Africa.

Mancotywa WS, 2001a, *First level analysis report: Phase 2 HVS testing of the Emulsion Treated natural gravel base section on road R2388 near Cullinan*, Contract Report CR-2000/47, CSIR Transportek, Pretoria, South Africa, South Africa.

Mancotywa WS, 2001b, *First level analysis report: 2nd Phase HVS testing of the Emulsion Treated Gravel and Foam Bitumen Gravel base sections on road P243/1 nearVereeninging*, Contract Report CR-2000/53, CSIR Transportek, Pretoria, South Africa, South Africa.

National Institute for Transport and Road Research (NITRR), 1986, *TMH1: Standard Methods of testing Road Construction Materials*, 2nd ed., CSIR, Pretoria, South Africa.

Otte E, 1972, *Die spannings- en vervormingseienskappe van sementgestabiliseerde materiale,* MSc dissertation, University of Pretoria, Pretoria, South Africa.

Otte E, 1978, *A structural design procedure for cement treated layers in pavements*, DSc thesis, University of Pretoria, Pretoria, South Africa.

Robroch S, 2001, *laboratory testing on foamed bitumen and cement treated material from the HVS test section on road P243/1*, Contract Report CR-2001/69, Transportek, CSIR, Pretoria, South Africa.

Semmelink CJ and Botha PB, 2000(a), *Evaluation of foam bitumen and emulsion treated ferricrete material on the new HVS site in the initial stages*, Contract report LR-2000/1/JR38794, Transportek, CSIR, Pretoria, South Africa.

Semmelink CJ and Botha PB, 2000(b) *Strength of foamed-cement and emulsion cement stabilised ferricrete base material from HVS site at Heidelberg as measured with K-mould*, Technical Report TR2001/14, Transportek, CSIR, Pretoria, South Africa.

Semmelink CJ, 2001, *Personal communication and correspondence*, Pretoria, South Africa.

Shackleton MC, 1995, *Modelling of the permanent deformation of untreated pavement layers*, MEng dissertation, University of Pretoria, Pretoria, South Africa.

Steyn WJvdM, 2001, *Level one data analysis of HVS tests on Foam Treated Gravel and Emulsion Treated Gravel on road P243-1: 80 kN and 100 kN test sections*, Contract report CR-2001/5, Transportek, CSIR, Pretoria, South Africa.

Theyse HL, 2000, *Laboratory design models for materials suited to labour-intensive construction: Volume I: Report*, Contract Report CR-99/038, Transportek, CSIR, Pretoria, South Africa.

Theyse HL, 2000, *The stiffness, strength and performance of unbound aggregate*, Contract report CR-2000/35, Transportek, CSIR, Pretoria, South Africa.

Van Vuuren H, 2001, *Personal communication and correspondence*, Bloemfontein, South Africa.

Verhaeghe BMJA, Napier RC and Kong Kam Wa NJ, 1998, *A Revised Approach to Mix Design of Emulsion Treates Base Materials: Laboratory Investigations*, Contract Report CR-97/057, CSIR Transportek, Pretoria, South Africa.

Verwey G, 2001, *Personal communication and correspondence*, Pretoria, South Africa.

Wolff H, 1992, *The Elasto-plastic behaviour of granular pavement layers in South Africa*, PhD thesis, University of Pretoria, Pretoria, South Africa.